Towards a Loophole-Free Bell's Inequality Experiment

Lin Yicheng Kelvin

An academic exercise presented in partial fulfilment for the degree of Bachelor of Science with Honours in Physics.

Supervisor: Professor Christian Kurtsiefer

Department of Physics

National University of Singapore

2011/2012

Acknowledgements

I express my greatest gratitude to my supervisor Professor Christian Kurtsiefer for the support and guidance throughout this project.

My thanks to my mentor, Siddarth K. Joshi, for the help and discussions that have made this project a fulfilling one for me.

Thanks to all experimentalists, especially Gleb Maslennikov and Chia Chen Ming, in the Quantum Optics group for all their help rendered, patiences, discussions and advices that enhanced my understandings and knowledge throughout this project. It was a privilege for me to work in the group and a pleasure for me to work with them.

My thanks goes out to Brenda Chng and Tan Peng Kian for all the help and tips on academic writing, presentations and TEX-ing.

On a personal note, I would like to thank my famliy members and Joy, for their constant love, support and always there for me throughout my hectic period of studies.

Abstract

A violation of Bell's inequality suggests an incompatibility of quantum mechanics with local realistic theory. An experimental violation of the Clauser-Horne-Shimony-Holt (CHSH) variant of the Bell's inequality has been performed. However, local realistic theory cannot be discounted because of experimental loopholes, namely the locality loophole and the detection loophole. In this thesis, we attempt to close the two loopholes at the same time in a photonic CHSH Bell's inequality experiment. To close the locality loophole we utilize the Pockels effect of a Lithium Niobate crystal to switch between measurement bases randomly within nanoseconds. To close the detection loophole we intend to implement a Transition Edge Sensor which has a detection efficiency of about 99 %. However, there remains mechanical and electronics issues that have to be resolved before performing an eventual loophole-free Bell's inequality experiment.

Contents

1 Introduction **1**

2 Background **5**

2.1 CHSH Bell's Inequality 5

2.2 Fast Polarization Switch for Closing the Locality Loophole 9

2.2.1 Rotation of the Polarization Plane 9

2.2.2 The Pockels Effect 11

2.2.3 Electronic Measurement Basis Switch 13

3 Experimental Setup **16**

3.1 Overview of Setup 16

3.2 Grating Stabilized External Cavity Diode Laser 16

3.3 Lithium Niobate Crystal Pockels Cell 18

3.3.1 Lithium Niobate Crystal 18

3.3.2 Setting Up of the Pockels Cell 19

3.3.3 Alignment with x and y Rotation Crystal Holder 21

3.3.4 Conoscopic Interference Patterns 22

3.4 Visibility Measurement 23

4 Results and Discussions **25**

4.1 Characterization of Lithium Niobate 25
4.1.1 Half-Wave Voltage and its Optical Axis 28
4.1.2 Electro-Optic Coefficient r_{22} 30
4.1.3 Rotation of the Polarization Plane at Low Voltages 32
4.1.4 Investigating the Fast Switching Capability 37

5 On Going and Future Work **44**
5.1 Minimzing the Piezoelectric Ringing 44
5.2 Closing the Detection Loophole - The Transition Edge Sensor 45

6 Conclusion **48**

Reference **50**

A Calculations **53**
A.1 CHSH Bell's Inequality 53
A.1.1 State Invariant of Measurement Basis 53
A.1.2 Probability Calculations 54
A.1.3 Derivation 54
A.2 Working of a Half-Wave Plate 56
A.3 Mathematics of Pockels Effect 58
A.4 Analyzer Intensity Dependency on Phase Difference 61

B Alignment Steps for Lithium Niobate **63**
B.1 Alignment With x and y Rotation Crystal Holder 63
B.2 Alignment Without x and y Rotation Crystal Holder 65

C Error Analysis **67**

C.1 Visibility Calculations 67

C.2 High Voltage Card 69

C.3 Error bars 70

C.3.1 Half-Wave Voltage Graph 70

C.3.2 r_{22} Linear Graph 71

C.4 Curve Fitting 71

C.5 Uncertainty in $n_o^3 r_{22}$ Determination 72

C.6 Other Experimentally Assigned Uncertainties 73

D Pictures of Experimental Setups **74**

Chapter 1

Introduction

Realism is the idea that particles have definite physical properties and they continue to have such properties whether or not these properties are measured [1]. In addition, the measurements should be local, in the sense that these physical properties should only be affected by their immediate surroundings. In 1935, Einstein, Podolsky and Rosen (EPR) hypothesized local realism in quantum mechanics [2]. In summary, they found it strange that in the quantum mechanical description of an entangled system of two particles, a measurement performed on one of the entangled particles, influences the value of the same physical quantity of a similar measurement on the other particle. They proposed that quantum mechanics was incomplete and could be missing some local hidden variables (LHV), which would cause such correlations in the particles, thus preserving the local realistic assumption. The idea of introducing a set of LHV to bring quantum mechanics neatly into the framework of classical physics is known as the LHV theories. About 30 years later in 1964, John Bell formulated a Bell's inequality based on a thought experiment which could probably rule out LHV theories [3]. In 1969, Clauser, Horne, Shimony and Holt (CHSH) extended this work to show that John Bell's analysis was applicable to actual physical systems as well. They presented a variant of the Bell's inequality, referred to

as the CHSH Bell's inequality [4]. Since then, many variants of the Bell's inequality have been proposed and their corresponding experiments performed. In 1972, Freedman and Clauser [5] were the first (and subsequently in 1982 by Alain Aspect [6]) to use entangled photons from atom cascades for such Bell's inequality experiments. Their experimental results violated Bell's inequality.

However, these experimental violations of Bell's inequality suffered from loopholes which allow interpretations using LHV theories. The loopholes in the Bell's inequality experiment are commonly classified into two types - the detection loophole and the locality loophole. The work by Ilja Gerhardt and Qin Liu demonstrates that both of these loopholes have to be closed at the same time in an experiment before the violation of the Bell's inequality can be seen as a rejection of LHV theories [7].

The first loophole is known as the locality loophole which arises from the fact that the measurements done on one of the entangled particles is influenced by the measurements conducted on the other particle. To close this loophole,we utilize the Pockels effect of a Lithium Niobate crystal to switch between measurement bases randomly within nanoseconds. More information about measurement bases are found in section 2.1.

The second loophole is known as the detection loophole, which arises as it is not possible to detect and measure all the entangled particles produced in an experiment. It can be argued that those detected particles could have already been pre-selected to give a result that violates Bell's inequality, and such a selection can be described by LHV. It is shown that for the CHSH inequality, the minimum detection efficiency is set at 82.8% [8]. This value is lowered down further to 66.6% using partially entangled states as shown by Eberhard [9].

To date, no experiment has yet to be performed that closes the two loopholes at the same time. There are two common ways of conducting Bell's inequality experiments - it could be carried out using two highly correlated atoms which could close the detection loophole, but fail

miserably with regards to closing the locality loophole. The work done by the group led by Rowe [10] was the first in closing the detection loophole with $^9Be^+$ atoms that were entangled in their transition states. However, closing the locality loophole in this case requires the separation of the ions apart while still preserving their states which proves experimentally challenging. The other common way of performing a Bell's inequality experiment is to use highly correlated photon pairs in which the locality loophole is closed [6, 11], but does not satisfactory close the detection loophole. This is because once the entangled photons are created, they propagate while preserving their individual state. As such, a wide separation between the two photons' detections with a random and fast time varying analyzer allows the locality loophole to be closed. However, accumulated losses in the photonic experiment makes closing the detection loophole challenging.

The goal of this project is to simultaneously close the locality loophole and the detection loophole in an experiment. To close the locality loophole, the measurement bases have to change fast enough in a nanosecond time range. We employ the Pockels effect of a Lithium Niobate crystal (LN crystal) to achieve a change in the plane of polarization of the detected photons, thus an equivalent change in the measurement bases is obtained. To close the detection loophole, the detection efficiency has to be as high as possible. A better single photon detection technique called the Transition Edge Sensor (TES) has been developed. The TES has a high reported detection efficiency of 99% [12] which seems promising in closing the detection loophole. Therefore, we will employ the TES to close the detection loophole. However, due to technical issues in getting the TES to work, this thesis would be heavily centered on developing a fast polarization bases switch used in closing the locality loophole.

In this thesis, we will introduce the background knowledge required in this project chapter 2. We will present the CHSH variant of the Bell's inequality formulation in a photonic experiment using entangled photons first. We will also highlight the importance of a fast measurement basis

switch in closing the locality loophole and how a fast measurement basis switch is done. We will also present the working principle of using the Pockels effect of a LN crystal in achieving a switch in the measurement basis. We show the practical implementation of the theory presented in chapter 2 in chapter 3. The experimental results on the properties of the LN crystal are presented in chapter 4. In chapter 5, we summarize the problems we have encountered and future work to be done.

Chapter 2

Background

In this chapter, we introduce CHSH Bell's inequality and show that to close the locality loophole in this formulation, we need to have a very fast switch between the two measurement settings for each receiving party of the entangled photon pairs. We also describe the utilization of a Pockels cell in implementing the fast switch.

2.1 CHSH Bell's Inequality

The Clauser-Horne-Shimony-Holt (CHSH) inequality is a variant of Bell's inequality that allows quantum mechanics and LHV theories to be distinguishable. To exemplify the CHSH inequality in a photonic experiment, let us look at a typical CHSH experiment setup as shown in figure 2.1. The CHSH experiment would first require a source that produces highly correlated photon pairs.

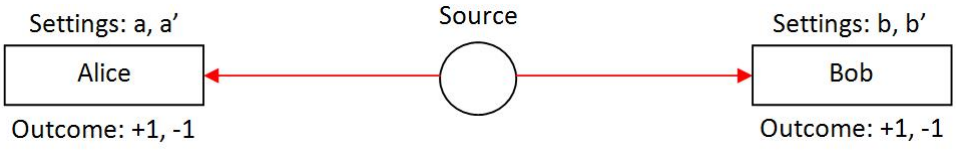

Figure 2.1: A schematic diagram of a CHSH experiment which requires two settings (a,a' or b,b') and two measurement outcomes (+1,-1) per setting.

The source produces photon pairs that are entangled in their polarization states. The photon pairs' polarizations are linear and orthogonal to each other. Since the photon polarization state has only two degrees of freedom, we term one polarization as *Horizontal* (H) and the other as *Vertical* (V). As such, a photon pair produced by the photon pair source could have the state,

$$|\Psi^-\rangle = \frac{1}{\sqrt{2}} \left(|H\rangle_1 \otimes |V\rangle_2 - |V\rangle_1 \otimes |H\rangle_2 \right) \tag{2.1}$$

Each photon is sent to one of two parties, namely Alice and Bob, for measurement. During the measurement of the correlated photon pairs, let us consider that Alice's photon enters a set of detectors I_a and Bob's photon enters a set of detectors II_b where a and b are adjustable experimental settings. Since any two orthogonal polarizations are sufficient in fully describing the polarization state of the light, the settings in our photonics experiment are the light polarization measurement basis such as the HV basis. In one such basis, the photon must take on binary outcomes, +1 or -1. For example, in the HV basis, the photon must either be in the H or V polarization and produces a respective click in the detector measuring the H or V polarization respectively. The outcomes for settings a and b for Alice and Bob are represented by $A(a)$ and $B(b)$ respectively. If a set of LHV, denoted as λ, governs the outcomes of the measurements, then the outcomes are deterministic functions $A(a, \lambda)$ and $B(b, \lambda)$. After repeating many measurements on the photon pairs, there is a joint conditional probability distribution $P(A, B|a, b, \lambda)$ for the outcome of A and B, given the settings a, b and λ,

$$P(A, B|a, b, \lambda) = P(A|a, \lambda)P(B|b, \lambda) \tag{2.2}$$

To retrieve $P(A, B|a, b)$, we average the joint conditional probability distribution over the prob-

ability distribution of λ, $f(\lambda)$,

$$P(A,B|a,b) = \int f(\lambda) P(A,B|a,b,\lambda)\,\mathrm{d}\lambda \tag{2.3}$$

The expectation value at settings a and b is defined as,

$$E(a,b) = P(+1,+1|a,b) + P(-1,-1|a,b) - P(+1,-1|a,b) - P(-1,+1|a,b) \tag{2.4}$$

From this, the CHSH inequality is obtained as shown in Appendix A.1.3,

$$\langle S \rangle = |E(a,b) + E(a,b') + E(a',b) - E(a',b')| \leq 2 \tag{2.5}$$

To look at the quantum mechanical description of the $\langle S \rangle$ value, the respective probabilities $P(A,B|a,b) = |\langle A(a)|_1 \langle B(b)|_2 |\Psi^-\rangle|^2$ can be shown in Appendix A.1.2 to be,

$$P(H,H|a,b) = P(V,V|a,b) = \frac{1}{2}\sin^2(a-b)$$

$$P(H,V|a,b) = P(V,H|a,b) = \frac{1}{2}\cos^2(a-b) \tag{2.6}$$

Substituting the probabilities in equations 2.6 into the expectation value in equation 2.4, we obtain

$$E(a,b) = -\cos 2(a-b) \tag{2.7}$$

Finally, substituting in the expectation values into the inequality of equation 2.5, as well as

choosing the following settings,

$$a = 0^\circ,\ a' = 45^\circ,\ b = 22.5^\circ \text{ and } b' = -22.5^\circ \tag{2.8}$$

we can show that,

$$\langle S \rangle_{QM} = 2\sqrt{2} \tag{2.9}$$

which violates the value of 2 as formulated using *any* LHV theory. Therefore, this shows that quantum mechanics is incompatible with any LHV theory and that quantum mechanics is nonlocal.

We return to the schematic diagram as shown in figure 2.1 to explain the physical realization of the measurement settings. The measurement settings would refer to the bases that are rotated by the respective angles in equation 2.8, with H defined as the polarization at 0°. The corresponding outcome of +1 or -1 would refer to the detector's click for the incoming photons with its plane of polarization parallel or perpendicular to the respective angles in equation 2.8. For example, setting $a = 0^\circ$ would mean measuring in the HV basis and a +1 would be a detector's click for seeing a photon in the H polarization. $a = 45^\circ$ refers to the $\pm 45^\circ$ basis, which is a rotation of 45° with respect to the HV basis and a +1 corresponds to detecting a photon polarized in the +45° plane. After performing the experiment over time, the detected particles are in a statistical distribution and the expectation value $E(a, b)$ would be

$$E(a,b) = \frac{N_{+1,+1} + N_{-1,-1} - N_{+1,-1} - N_{-1,+1}}{N_{+1,+1} + N_{-1,-1} + N_{+1,-1} + N_{-1,+1}} \tag{2.10}$$

where N_{AB} is the total number of coincidence pairs of the respective outcomes A and B, where A and B each take on the binary outcomes +1 or −1. It follows that we can obtain the

experimental $\langle S \rangle$ value by substituting the expectation values obtained through equation 2.10 in equation 2.5. If we are successful in closing the loopholes and still obtaining an $\langle S \rangle$ value of more than two, then the LHV theory is rejected.

2.2 Fast Polarization Switch for Closing the Locality Loophole

2.2.1 Rotation of the Polarization Plane

For closing of the locality loophole, the two measurement bases each for both Alice (a and a') and Bob (b and b') mentioned in section 2.1 would need to change fast enough. By 'fast', we mean that Alice's measurement basis change must be completed before information on Bob's measurement in a corresponding basis reaches Alice. Consider a simple example where only three photon pairs are detected. At a particular time t, both Alice and Bob start their measurements at settings a and b on the first photon pair. Information of their measurements at settings a and b would start to travel towards each other. After some time $t + \tau$, when the measurement information of Alice has reached Bob and that of Bob has reached Alice, the first photon pair must have its measurement completed and the second photon pair will be measured in a new random basis. It follows that by the time $t + 2\tau$, the measurement basis must have been changed again to measure the third photon pair. This indicates that the change in the measurement basis must be done within time interval τ.

To look at how a change in the measurement basis is done, we first look at how measurements in different bases are conducted in an experiment. Figure 2.2 shows how we perform measurements in HV basis and $\pm 45^\circ$ basis (settings a and a'). As shown in figure 2.2, to measure in the HV basis, we allow incoming photons to pass through a Polarization Beam Splitter (PBS) and measure the intensity on the transmitted and reflected beam. Generally, a PBS separates an incident light beam into two orthogonal linear polarizations in the transmitted and

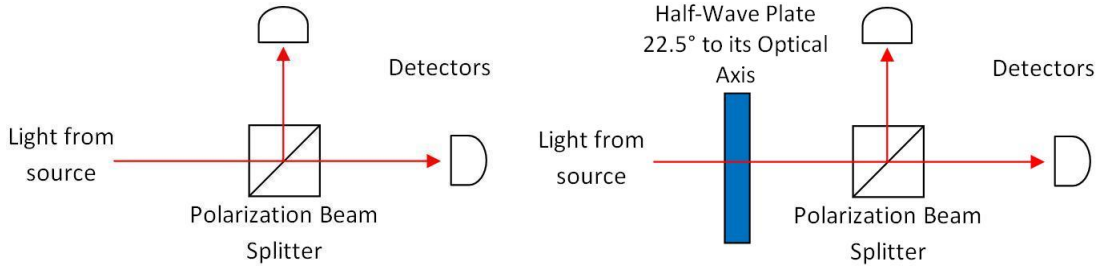

Figure 2.2: Left: Measurement in the HV basis. Right: Measurement in the $\pm 45°$ basis. A polarization beam splitter separates input light into two orthogonal linear polarizations in the transmitted and reflected beams. A change of measurement settings between $a = 0°$ and $a' = 45°$ would mean changing from the setup on the left to the setup on the left, or alternatively just using the setup on the right and rotating the half-wave plate from $0°$ to $22.5°$ to the optical axis.

reflected beams. The transmitted and reflected beams can be assigned H and V polarizations respectively. To measure in the $\pm 45°$ basis, we rotate the polarization of the incident light by $45°$ before passing the incoming photons through a PBS. We rotate the polarization plane by placing a half-wave plate at $22.5°$ with respect to the optical axis. The mathematical description of the workings of the half-wave plate is presented in Appendix A.2. A change of measurement settings from $a = 0°$ to $a' = 45°$ would mean a rotation of the plane of polarization of incoming photons from $0°$ to $45°$. It follows that such a rotation must be done within a short interval of time τ.

In this project, we control the rotation from one plane of polarization to another by $45°$ for a change in the measurement settings electronically. Even though it could be done mechanically by rotating a half-wave plate in front of a PBS from $0°$ to $22.5°$, such a mechanical change is too slow. To illustrate how fast the measurement settings would have to change, let us place the detectors be placed approximately 2 m apart. If we assume that information about the measurement travels at the speed of light, we then require a change in the measurement settings within nanoseconds. In the next section 2.2.2, we show how we achieve an electronical switch in the measurement bases by utilizing a Pockels cell.

2.2.2 The Pockels Effect

In order to understand how a fast polarization rotation switch works, we start off by discussing the working mechanism of the Pockels cell - the Pockels effect.

When an optical light beam passes through a material, the speed of the light through the material changes. The refractive index n of a material is defined as the ratio of the speed of light in vacuum to the speed of light in the material and it depends on the wavelength of the incident light as well as its polarization plane. For example, when linearly polarized light, that has its electric field oscillating in just one direction, passes through a birefringent crystal, orientated 45° to the crystal's optical axis, the light splits into two as shown in figure 2.3. The light from

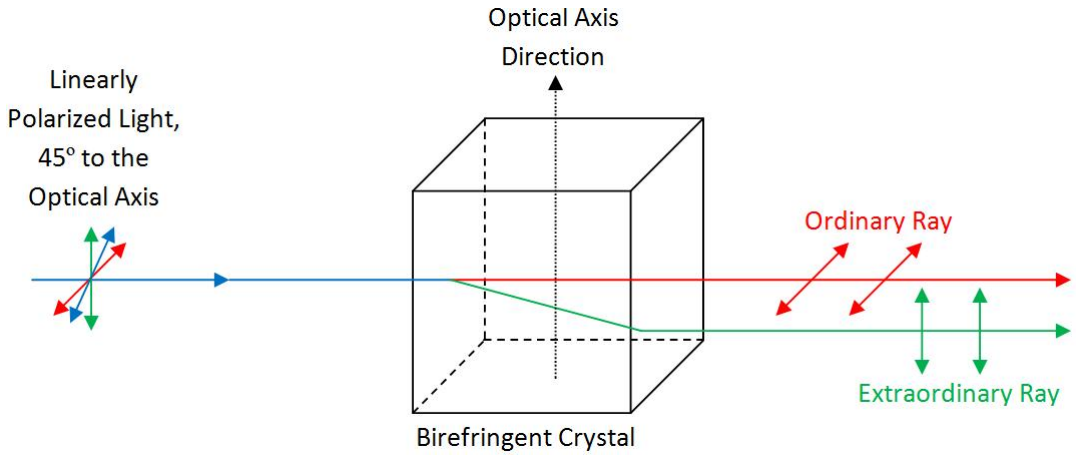

Figure 2.3: The separation of a linearly polarized light into two paths of orthogonal planes of polarization when passing through a birefringent crystal.

each path is still linearly polarized and the plane of polarization of the extraordinary ray (e-ray) and ordinary ray (o-ray)are orthogonal to each other. One of the planes of polarization is parallel to the optical axis, while the other is perpendicular to the optical axis. The difference in the refractive index of the e-ray and the o-ray is known as the birefringence of the material. Furthermore, in some materials, when an electric field is applied across them, the refractive index of the materials changes according to the strength and direction of the applied electric field. Such an effect is known as the electro-optic effect.

The electro-optic effect is a well-known observable phenomenon. In 1875, Reverend John Kerr observed that any clear material became birefringent under a static external electric field [13]. This effect is known as the Kerr effect, where the refractive index of the material varies with the applied electric field strength in a quadratic manner. In 1893, Friedrich Carl Alwin Pockels observed that the birefringence of a crystal varies linearly with the applied electric field for a crystal that lacks inversion symmetry, [14]. This linear change of birefringence Δn due to an applied electric field E_2 was later known as the Pockels effect,

$$\Delta n = \left(n_{x_1'}^{'} - n_{x_2'}^{'} \right) = n_o^3 r_{22} E_2 \tag{2.11}$$

where $n_{x_1'}^{'}$ and $n_{x_2'}^{'}$ represent the refractive indices of the e-ray and the o-ray respectively when passing through the LN crystal with an applied electric field. The n_o is the refractive index of the o-ray when there is no applied electric field and r_{22} is known as the electro-optic coefficient of the crystal used. The rigorous mathematics leading to equation 2.11 can be found in Appendix A.3. The phase difference Γ between the e-ray and the o-ray is then defined as

$$\Gamma = \frac{2\pi}{\lambda} \Delta n L = \frac{2\pi}{\lambda} n_o^3 r_{22} E_2 L \tag{2.12}$$

$$\Gamma = \pi \cdot \frac{V}{V_\pi} \tag{2.13}$$

with the so-called half-wave voltage,

$$V_\pi = \frac{\lambda}{2 n_o^3 r_{22}} \cdot \frac{d}{L} \tag{2.14}$$

where V is the applied voltage across the crystal with thickness d, and L is the length of the

crystal along the propagation of the light. Equation 2.12 tells us that the phase difference between the e-ray and the o-ray scales proportionally with the applied electric field. When we apply the half-wave voltage, we find that the phase difference between the e-ray and the o-ray is π.

2.2.3 Electronic Measurement Basis Switch

.

A Pockels cell is an electronically controlled half-wave plate consisting of an electro-optical crystal in between a pair of electrodes. For our Pockels cell, the output photon polarization plane is rotated 45° with respect to an input photon polarization plane. Let us consider that the input linear polarization is orientated 22.5° with respect to the electro-optical axis created once a voltage is applied across the crystal. If the input linear polarization is labelled as H polarization, it will be rotated by 45° to to give us +45° polarization light at the output as shown in figure 2.4. If we rotate the plane of linear polarization of the input light to +45°

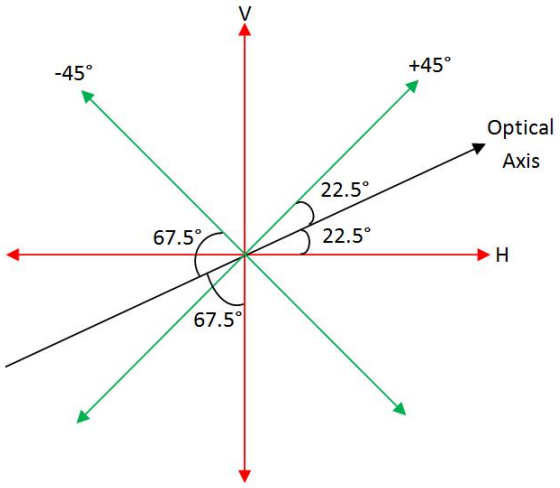

Figure 2.4: A picture showing the H and V polarizations, the +45° and −45° polarizations and the respective angles they make with the optical axis. It follows that in such a setting, H and V polarizations are rotated to +45° and −45° polarizations respectively and vice versa.

without changing the alignment of the LN crystal, it will make an angle of −22.5° with respect

to that electro-optical axes and gets rotated back to H polarization. Table 2.1 summarizes the output light polarization for different applied voltages when input light with different linear polarizations enter the LN crystal.

Table 2.1: Summary of output polarization with different input polarization at different applied voltages.

	Output Polarization	
Input Polarization	Applied Voltage Across the Crystal	
	0 V	Half-wave Voltage
$\|H\rangle$	$\|H\rangle$	$\|+\rangle$
$\|V\rangle$	$\|V\rangle$	$\|-\rangle$
$\|+\rangle$	$\|+\rangle$	$\|H\rangle$
$\|-\rangle$	$\|-\rangle$	$\|V\rangle$

where in the normalized *Jones Vector* representation,

$$|H\rangle = \begin{pmatrix} 1 \\ 0 \end{pmatrix}, |V\rangle = \begin{pmatrix} 0 \\ 1 \end{pmatrix}, |+\rangle = \frac{1}{\sqrt{2}} \begin{pmatrix} 1 \\ 1 \end{pmatrix}, |-\rangle = \frac{1}{\sqrt{2}} \begin{pmatrix} 1 \\ -1 \end{pmatrix} \tag{2.15}$$

describing Horizontal, Vertical, $+45°$ and $-45°$ polarizations respectively.

A modified setup for the two measurement bases using the Pockels cell is shown in figure 2.5. As shown in figure 2.5, when there is no voltage supplied, there is no rotation of the plane of

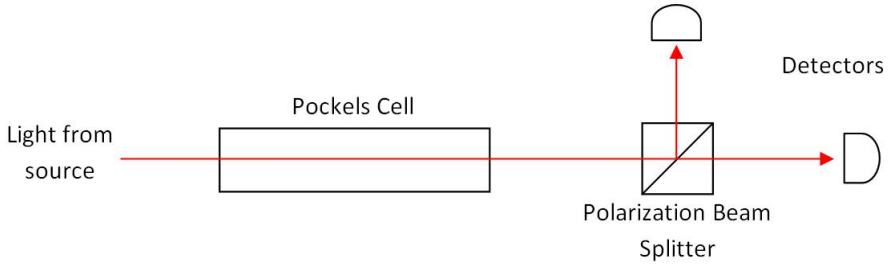

Figure 2.5: A schematic diagram of using a Pockels cell to perform measurements in the two bases. Measurement in one of the bases takes place when no voltage is applied to the Pockels cell. Measurement in the other basis happens when a half-wave voltage is applied to the Pockels cell.

polarization of the light and the setup will be measuring in the HV basis. When the switching voltage is applied, a rotation of $45°$ occurs and the setup would measure the light in the $\pm 45°$

basis. Therefore, a rotation of incoming photon's plane of polarization electronically can be attained.

We note that in order to close the locality loophole, it is insufficient just to have a fast polarization switch. The switch in the measurement bases must be done randomly such that the experimentalists carrying out the experiment must not know at any one time, which basis they are measuring. This is to eliminate any local effect on the experiment due to the actions of the experimentalists. As such, the switching between voltages will be controlled by a random signal generator so that at any one time, the experimentalists do not know when and which basis the detectors are measuring. It is only after the experiment has been performed, when the total number of coincidence counts at each measurement basis is tallied, we can then calculate the $\langle S \rangle$ value.

In the next chapter, we present the detailed experimental investigations of the feasibility of using an LN crystal as an electronic measurement basis switch.

Chapter 3

Experimental Setup

In this chapter we present the experimental details of setting up the components required for using the Pockels cell as a fast measurement basis switch. We briefly described about the external cavity laser used to characterize and align the Pockels cell. We also describe the alignment procedure and measure the visibility.

3.1 Overview of Setup

The description of the setup shown in figure 3.1 can be divided into the two sections - the laser light source that provides a stable and narrow bandwidth laser light of $\leq$10 MHz and the LN crystal setup.

3.2 Grating Stabilized External Cavity Diode Laser

A grating stabilized external cavity diode laser was set up to provide a narrow bandwidth laser beam at 806 nm with low output power fluctuations for characterizing the LN crystal. The external laser cavity is important in our analysis since the electro-optic effect depends on the

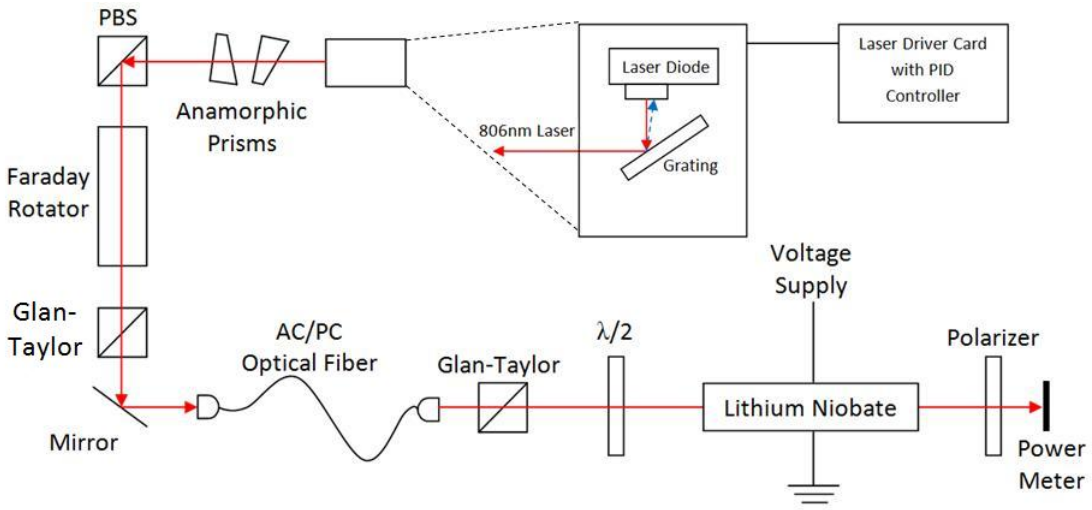

Figure 3.1: A overview schematic diagram of our experimental setup. Note that the angle-cut (AC) end of the optical fibre is facing the laser source.

wavelength of the input light as seen from the half-wave voltage equation 2.14. Figure 3.2 shows the setup of the laser source and the insert shows the details in the external laser cavity.

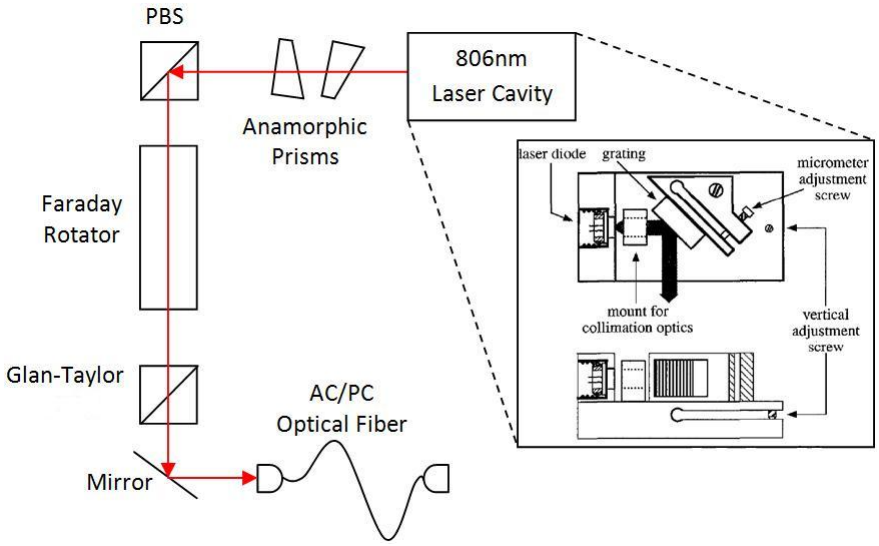

Figure 3.2: A schematic diagram of the external laser source, with insert showing details in the external laser cavity [15].

An aspheric lens of focal length about 4.5 mm (Thorlabs C230-TME B) was used to collimate the divergent light out of a 806 nm laser diode. A diffraction grating of 1800 lines per millimeter was then placed in a Littrow configuration such that the first order of the diffraction of the

collimated light was reflected back into the laser diode to enhance lasing for a narrow bandwidth.

A home-made driver board supplies the current and maintains the temperature of the laser diode. The temperature was maintained by a Proportional-Integral-Derivative (PID) controller which was connected to a Peltier element mounted below the laser diode stage. The PID controller maintains the temperature at a desired value. The current and temperature of the laser diode was set at around 131 mA and 24 °C respectively.

It is seen from figure 3.2 that the laser beam passes through a PBS, a faraday rotator and then a Glan-Taylor polarization beam splitter (which is essentially a type of PBS). This combination of optical components acts as an optical isolator that prevents back reflection of the laser light from getting into the laser diode, thus increases the power stability of the output beam. Lastly, the laser light was coupled into the AC end of a AC/PC (Angle-Cut/Plane-Cut) optical fibre via an aspheric lens with 4.5 mm focal length (C230-TME B lens). The AC/PC fibre served two purposes - it minimized the back reflection of the laser light at the AC surface and prevented internal and multiple back reflections in a normal PC (Plane Cut) optical fibre that might cause intensity fluctuations.

3.3 Lithium Niobate Crystal Pockels Cell

3.3.1 Lithium Niobate Crystal

The LN crystal is a negative uniaxial crystal and is cut such that its optical axis is along the z principle axis of the crystal. Light that is polarized parallel to the optical axis will travel slower than light that is polarized perpendicular to the optical axis. This intrinsic birefringence effect could be undesirable in our experiment and therefore, the alignment of the LN crystal such that the light propagation path is parallel to the optical axis of the crystal is important to minimize or even eliminate the effect of the intrinsic birefringence of the crystal from interfering with the

results.

The LN crystal belongs to the trigonal crystal symmetry with the class of R3c and has a point group of 3m which means that the LN crystal lacks an inversion symmetry. An inversion symmetry would tell us that an equal but opposite electric field, $\hat{E}$ and $-\hat{E}$, would have the same effect on the electronic structure of the crystal. As such, the change in the refractive index of a crystal with an inversion symmetry would be the same for equal and opposite electric fields. This is not the Pockels effect because a negative applied electric field would have different effect from a positive applied electric field across the crystal. Therefore, Pockels effect can only be observed in crystals that lack an inversion symmetry.

Most of our 806 nm light would pass through the crystal as it is transparent from 400 nm to 5000 nm [16]. However, we do note from the start of the project that the LN crystal is generally piezoelectric, where an applied voltage across the crystal would change the dimension of the crystal. In addition, the LN crystal has strong acousto-optical responses where acoustic waves in the crystal changes its refractive index. Throughout this project, we also investigate how such responses would affect the outcome of the light after the Pockels cell, and whether or not such effects limit our ability to perform a loophole free Bell's inequality experiment.

3.3.2 Setting Up of the Pockels Cell

There are basically two types of Pockels cell, depending on the way in which we apply the electric field across the crystal as shown in figure 3.3. In a transverse Pockels cell, the applied electric field is perpendicular to the propagation of the light beam through the crystal, whereas in a longitudinal Pockels cell, the applied electric field is parallel to the propagation of the light beam through the crystal.

There are different advantages between the two types of Pockels cell. In the longitudinal arrangement, $d = L$ in equation 2.14. Therefore, the birefringence is only sensitive to the voltage

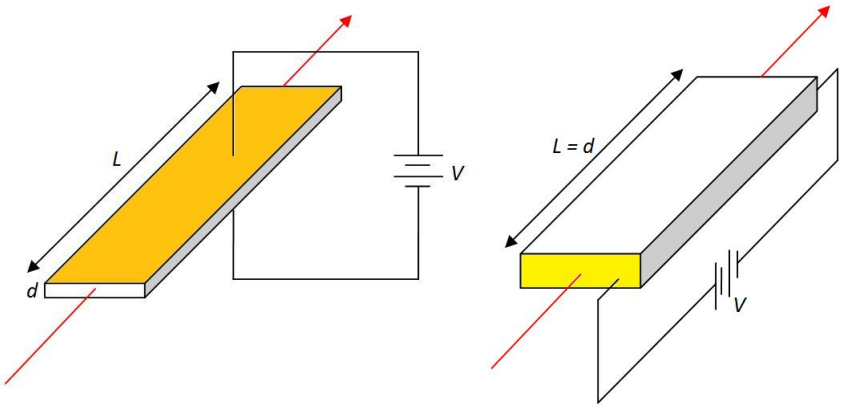

Figure 3.3: Schematic diagrams of a Left: Transverse Pockels Cell. Right: Longitudinal Pockels Cell.

applied. As such, the dimension of the crystal can be varied to have a wide opening window for the light beam to pass through the crystal. This increases its field of view and reduces losses due to clipping of the light. However, it is not applicable for a fast switch as the half-wave voltage is too high and the power generated during the switch is too great for current electronics to dissipate. For a fast switch, a low half-wave voltage for our crystal is desirable, thus a transverse configuration where the birefringence is also affected by the thickness to length ratio $\frac{d}{L}$ of the crystal is preferred. The smaller the ratio, which implies smaller d and/or larger L, the smaller is the half-wave voltage. Nevertheless, d cannot be too small as there will be substantial loss due to clipping since the window that the light can pass through is smaller. However, neither can L be too large since a homogeneous crystal with large L is not only difficult to find, but it also poses difficulty in the alignment of the crystal. In this project, we will be using a LN crystal of dimensions $1.5 \times 10 \times 100$ mm, where $d = 1.5$ mm and $L = 100$ mm.

The alignment of the crystal would depend on the degrees of freedom in rotating the crystal with respect to a light beam. There are two different holders used to place the LN crystal in this project. We used the first holder, which we had rotational degrees of freedom in the x and y axes (rotation in p and q) of the crystal, to determine the half-wave voltage and the electro-optical axis. For the second holder, which has no rotational degree of freedom, was used

to investigate the fast switching capability of the crystal.

3.3.3 Alignment with x and y Rotation Crystal Holder

The step-by-step procedure for aligning the LN crystal are detailed in Appendix B.1. The LN crystal in this holder was held in place by clamping it with a copper plate and two screws. The output light beam from the external laser cavity was coupled into a single mode fibre and the output of the fibre is collimated using an aspheric lens with focal length of about 4.5 mm (Thorlabs C230 TME B) and passed through a Glan-Taylor polarizer, where the output light beam was defined to be in the H polarization. Without the LN crystal in the light path, we made the light beam approximately parallel to the optical table by passing the beam through two pinholes at equal heights. It was ensured that there was sufficient space in between the two pinholes as the LN crystal and its holder will be placed in between the two pinholes. After which, the LN crystal was placed in the light path and while the second pinhole was closed. The output light from the crystal was checked to pass through the pinhole approximately, to ensure that the light beam was not bent due to coarse misalignment of the crystal. After which, both pinholes were opened for fine alignment of the crystal. A polarizer was placed at the end of the two pinholes, 90° with respect to the H polarization of the light to look for a minimum intensity after the polarizer was measured on a power meter.

For the fine alignment of the crystal, since the polarizer was orientated at cross-polarization to the initial light beam, the intensity should also be at the minimum when the crystal was in place. The crystal was rotated about the y-axis, which is perpendicular to the optical table, to find a global minimum intensity. This would ensure that the birefringence axis lies in the yz plane of the crystal. Next, the power meter was removed and a camera (without lens) was placed at the back to observe the light through the crystal. The polarizer was also shifted to the front of the crystal to minimise the intensity of the light reaching the camera such that the

camera would not saturate. Any clipping of the light due to the crystal would be seen in this manner. The crystal was then rotated about the x-axis so as to get a nice beam profile, which was approximately circular in shape without clipping, on the camera. Then, the conoscopic interference pattern was looked for, which will be discussed later in section 3.3.4.

After the conoscopic interference pattern was observed, fine adjustment in the x-axis rotation was performed if necessary. A half-wave plate at 22.5° was placed before the crystal. The polarizer was then placed at $-45°$ such that it was at cross-polarization with the input light polarization. The x-axis rotation was finely adjusted so as to get a global minimal intensity at the output. The camera without lens was also placed at the end of the polarizer and served as a check on the beam profile, since the clipping will also cause a reduction in beam's intensity. Lastly, we sent a voltage across the crystal and a change in the output intensity after a polarizer indicates that the light beam has indeed being passed through the crystal.

3.3.4 Conoscopic Interference Patterns

When a diverging light beam is passed through a uniaxial crystal along its intrinsic optical axis (which is the z-axis of the LN crystal), an interference pattern in the form of a 'maltese' cross pattern is seen. Figure 3.4 shows the conoscopic interference pattern that we have obtained in our LN crystal.

The conoscopic interference pattern obtained tells us that the LN crystal is indeed unaxial and z-cut, where the propagation of the light is along the z-axis of the crystal. If the crystal is properly aligned, where the propagation of the light beam through the crystal is parallel to the z-axis of the crystal, the intensity of the four bright portions should be of the same shape and intensity. To get the interference pattern, we placed a cellulose tape in front of the crystal holder to diverge the light entering the crystal. The light after the polarizer, which was still at cross-polarization with the input light beam. A screen was placed after the polarizer and a

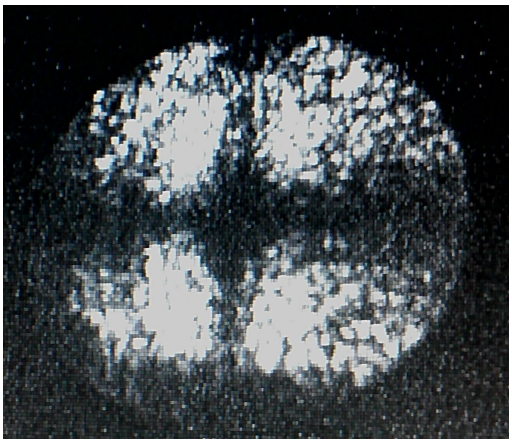

Figure 3.4: The experimental conoscopic interference pattern through the LN crystal, showing a distinct 'maltese' pattern with the dark crossed bands known as isogyres.

camera (with lens) was used to observe the pattern on the screen.

3.4 Visibility Measurement

Visibility is a measure of the degree of polarization of photons. Using the external cavity diode laser as the source after passing through a PBS, we know that the input laser beam polarization is linear with high visibility. By measuring the visibility of the laser beam after the crystal, we can get a estimate of how well we have aligned our crystal with respect to the laser light. To determine the visibility, incoming photons were passed through a polarizer which was then rotated for 360° and the intensities at various angular positions of the polarizer were noted. The visibility is defined as,

$$\text{Visibility} = \frac{I_{max} - I_{min}}{I_{max} + I_{min}} \tag{3.1}$$

For a perfect linearly polarized light, the visibility of 100 % while for a perfect circularly polarized light, it is 0 %. To determine the I_{max} and I_{min} experimentally, we plot the graph of light intensity against angular position of the polarizer as shown in figure 3.5. The graph was fit to

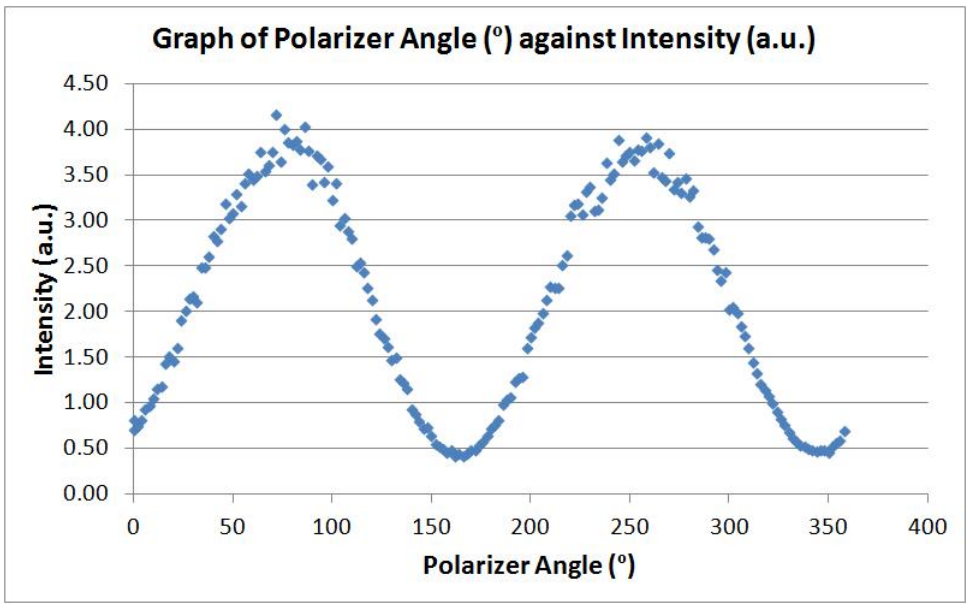

Figure 3.5: Visibility graph of voltage (V) against polarizer angle (°) which gives us the visibility of the light. The voltage here would be directly proportional to the intensity of the light.

identify the I_{max} and I_{min}. A sample of the visibility curve fitting is discussed in Appendix C.1.

Chapter 4

Results and Discussions

In this chapter, we characterize the LN crystal by finding its half-wave voltage and its optical axis. Since the half-wave voltage was found to be too high for efficient switching, we investigate how the crystal would perform at low applied voltages. We also calculated the electro-optic coefficient r_{22} for the LN crystal at 806 nm. We next examine the fast switching performance of the LN crystal at such low applied voltages.

4.1 Characterization of Lithium Niobate

In this section we determine the half-wave voltage and the electro-optical axis of the LN crystal. Incoming photons with polarization set at 22.5° to the electro-optic axis to the crystal will have its polarization rotated by 90°, thus executing a change in basis in our measurement. From mathematical calculations detailed in Appendix A.3, under an applied electric field to the LN crystal in the y direction, the electro-optical axes is approximately in the same directions as the original principle axes of the LN crystal, and thus we look for the half-wave voltage in a setup shown in figure 4.1.

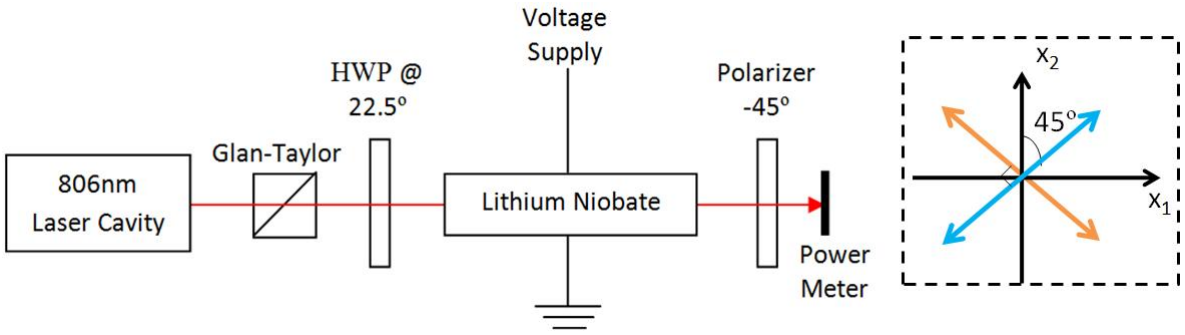

Figure 4.1: A schematic diagram of the setup to determine the half-wave voltage of the crystal. The external laser cavity is simplified to just a box in this diagram. The insert on the right shows the predicted electro-optic axis of the crystal, which boundary is represented by the dotted box. The blue arrow shows the direction of the linearly polarized light input and the orange arrow shows the direction of the polarizer axis in this setup.

The light from the external laser cavity was made to pass through a Glan-Taylor polarizer where the light was linearly polarized along the optical table, perpendicular to the propagation of the light. The light polarization plane was rotated by 45° using a half-wave plate at 22.5° with respect to the polarization of the light. This way, when a voltage was applied to the crystal, this linearly polarized light was decomposed into the e-ray and o-ray in equal weights. A polarizer was placed after the crystal such that the polarizer axis was orthogonal (at cross-polarization) to the polarization of the input light as shown by the orange arrow in the insert in figure 4.1. The light intensity after the polarizer was measured by a power meter. The power meter used was a photodiode connected in a circuit as shown in figure 4.2. When light falls on the photodetector,

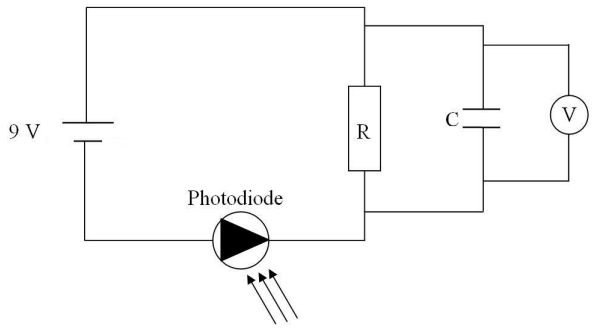

Figure 4.2: A schematic of the photodetector using voltage as a measurement of laser beam's intensity.

the photocurrent produced decreases the resistance of the photodiode. A suitable resistor is chosen such that the voltage across it is approximately proportional to the intensity of the light incident upon the detector. This ensures that the maximum voltage reading did not reach 9 V as the circuit will be saturated. A capacitor was used to act as a low-pass filter that stabilizes the voltage reading. It is to note here that the absolute intensity or power of the light was immaterial since we were only interested in the relative intensity of the output light with the maximum value that the photodiode can detect without saturation. A high voltage output card was used to supply the voltage across the LN crystal. The characterization of the high voltage card can be found in the Appendix C.

In the setup above, we look for the half-wave voltage in the following way. Malus law states that the intensity I of the light after the polarizer is given by

$$I = I_0 \cos^2 \theta \tag{4.1}$$

where I_0 is the maximum intensity obtainable through the polarizer and θ is the angle between the plane of linear polarization of the light and the polarizer axis. The polarizer axis is at 90° with respect to the polarization of the light. When there is no voltage applied to the LN crystal, the light polarization remains the same at the output. The intensity after the polarizer is therefore minimum experimentally (or in fact zero theoretically as $\theta = 90^\circ$).

However, when a voltage is applied to the crystal increases to the half-wave voltage, a plane of polarization flips of 90° takes place, where θ becomes 0°, a maximum intensity is obtained. To make it more mathematical, it can be shown in Appendix A.4 that the intensity after the polarizer is related to the phase difference Γ of the e-ray and the o-ray by,

$$I = I_0 \sin^2 \frac{\Gamma}{2} \tag{4.2}$$

Substituting equation 2.12 for the phase difference Γ in equation 4.2, it can be written as,

$$\frac{I}{I_0} = \sin^2\left[\frac{1}{2}\cdot\frac{2\pi}{\lambda}n_o^3 r_{22}\frac{L}{d}\cdot V\right] \tag{4.3}$$

From equation 4.3, we can see that the voltage at which we obtain the maximum intensity is known as the half wave voltage. The left hand side of equation 4.3 essentially tells us that the normalized intensity is more important than the absolute power, as the result will be insensitive to the intensity output of our external laser cavity, as long as there are no huge power fluctuations in the intensity.

4.1.1 Half-Wave Voltage and its Optical Axis

After varying the applied voltages and observing the respective intensity outputs, the graph of normalized intensity $\frac{I}{I_0}$ against the voltage V applied is plotted as shown in figure 4.3.

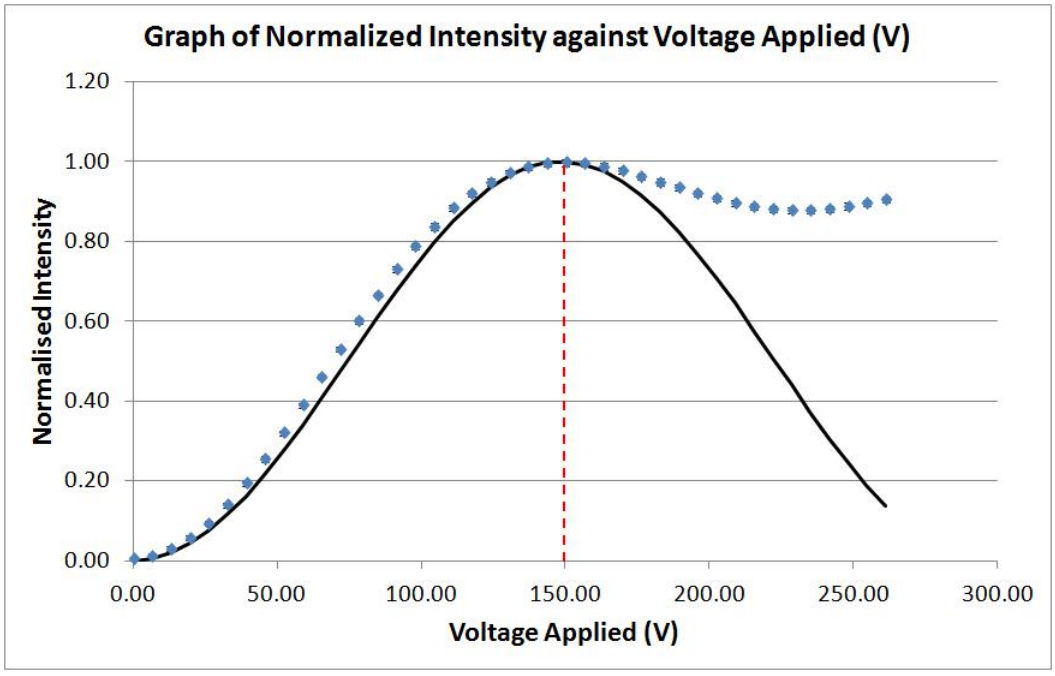

Figure 4.3: The graph of normalized intensity against the voltage applied (V) across the crystal. The blue points are the experimental data while the black curve is the theoretical fit of the data. The half-wave voltage of (150 ± 6) V is obtained at the point where the normalized intensity reaches the maximum. Note that the error bars are too small to be shown on the graph.

The experimental data points are shown in blue in the graph of figure 4.3. The black curve is a theoretical result of how the output light should behave. From the graph in figure 4.3, it is seen that the behaviour of the experimental normalized intensity output follows the $\sin^2$ behaviour as described in equation 4.3 until the voltage which gives us the highest normalized intensity at about (150 ± 6) V. However, the LN crystal started to deviate from the theoretical curve at high voltages. It is suspected that when the voltage is too high, the quadratic Kerr effect dominates which causes the deviation from the Pockels effect. It is not the focus in this project to understand the Kerr effect primarily because the voltage to utilize the Kerr effect for a nanosecond switch is too high. Therefore, we shall not be bothered by the deviation at high voltages. A statistical χ^2 test was done with 23 data points (before the deviation perhaps due to Kerr effect) as described in Appendix C.4 to quantify the fit of the curve. The value of $\chi^2 = 0.097$ which is smaller than 35.17 at 95 % confidence interval. Thus, it is consistent with the conclusion that our experimental result is a good fit with the theoretical behaviour.

The focus would be at the highest normalized intensity of about (0.998 ± 0.008) at the voltage of about (150 ± 6) V. The visibilities of the output light after the polarizer at 0 V and at (150 ± 6) V were compared to be (94 ± 1) % and (95 ± 1) % respectively. The uncertainty in the half-wave voltage is due to the fact that when a voltage between 144 V to 156 V was applied to the crystal, the power meter was not sensitive enough to show any observable change. This shows that the two visibilities are preserved and that there is a flip in the plane of polarization of the light beam by 90°. In addition, these results are also consistent with our guess that the electro-optic axis created is in the same orientation as that shown in figure 4.1 and that (150 ± 6) is the half-wave voltage. Since the half-wave voltage was obtained, our guess about the electro-optical axis was correct and the crystal is cut in the correct orientation that we want.

4.1.2 Electro-Optic Coefficient r_{22}

Since we have a narrow bandwidth source at 806 nm, our setup gives gives us an experimental electro-optic coefficient, r_{22} value at 806 nm. From equations 4.2 and 4.3, it is clear that,

$$\sin^{-1}\sqrt{\frac{I}{I_0}} = \frac{1}{2}\cdot\Gamma = \frac{1}{2}\cdot\frac{2\pi}{\lambda}n_o^3 r_{22}\frac{L}{d}\cdot V \tag{4.4}$$

Therefore, it follows that,

$$2\sin^{-1}\sqrt{\frac{I}{I_0}} = \Gamma = \frac{2\pi}{\lambda}n_o^3 r_{22}\frac{L}{d}\cdot V \tag{4.5}$$

Equation 4.5 basically gives us an experimental value to the phase difference Γ on the left hand side of equation 2.12 that describes the Pockels effect. Therefore, we went further to draw a linear graph of Γ (rad) against the applied voltage V, with a correlation coefficient value of 0.998 as shown in figure 4.4. The linear graph implies that the proportionality dependence of the phase difference to the voltage applied is observed in this project and that we are indeed looking at the Pockels effect of the LN crystal. The gradient of the straight line graph would give the r_{22} values. The gradient m of the curve gives,

$$m = \frac{2\pi}{\lambda}n_0^3 r_{22}\frac{L}{d} = (0.0210 \pm 0.0002)\ \text{rad V}^{-1} \tag{4.6}$$

There is no previous experimental determination of the refractive index at 806 nm can be found. Therefore, the Sellmeier equation used to calculate the refractive index of LN crystal at 806 nm is used. The Sellmeier equation is given by,

$$n_o = \left[A + \frac{B}{\lambda^2 + C} + D\lambda^2\right]^{1/2} \tag{4.7}$$

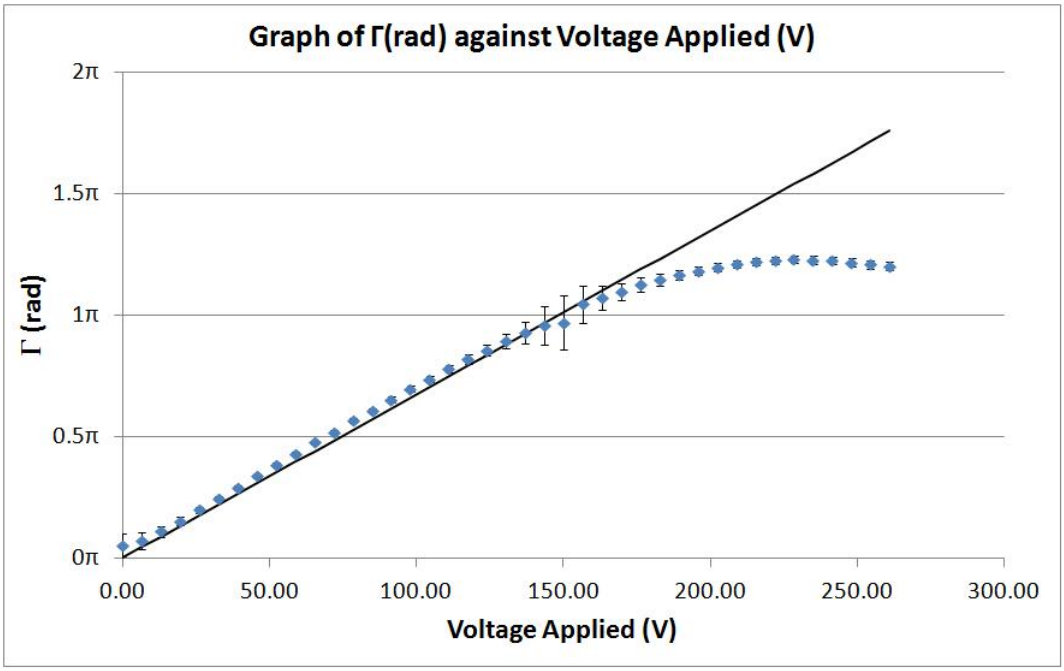

Figure 4.4: The graph of phase difference (rad) of e-ray and o-ray against the voltage (V) applied across the crystal. Again, the blue points are the experimental data while the black linear line is a linear fit for the range that obeys the Pockels effect. From the graph, the linear Pockels effect is observed.

where λ is the wavelength of the incident light and A, B and C are the experimental Sellmeier equation constants that are specific to respective crystals. It has been shown through the work in [17, 18] that the empirical Sellmeier equation constants for the LN crystal are,

$$A = 4.9048, B = 0.11768\ \mu\text{m}^2, C = -0.0475\ \mu\text{m}^2, D = -0.027169\ \mu\text{m}^{-2} \tag{4.8}$$

when the wavelength λ is measured in μm. With the constants in 4.8 and equation 4.7, the refractive index is calculated to be,

$$n_o = 2.254 \pm 0.002 \tag{4.9}$$

The product of the cube of refractive index and the electro-optical coefficient is,

$$n_o^3 r_{22} = (4.1 \pm 0.1) \times 10^{-11} \text{ mV}^{-1} \tag{4.10}$$

Taking the refractive index value in equation 4.9, the experimental value for the electro-coefficient, r_{22} for a clamped LN crystal of light beam at 806 nm is,

$$r_{22} = (3.5 \pm 0.1) \times 10^{-12} \text{ m V}^{-1} \tag{4.11}$$

4.1.3 Rotation of the Polarization Plane at Low Voltages

We have determined the half-wave voltage to be (150 ± 6) V. However, it is still too high for an effective switch at high frequency. The switching cannot be done by switching on and off a power supply. It has to be done electronically using a 100 V BLF573 transistor as shown in a circuit diagram below in figure 4.5. The high power supply shown in figure 4.5 can take two

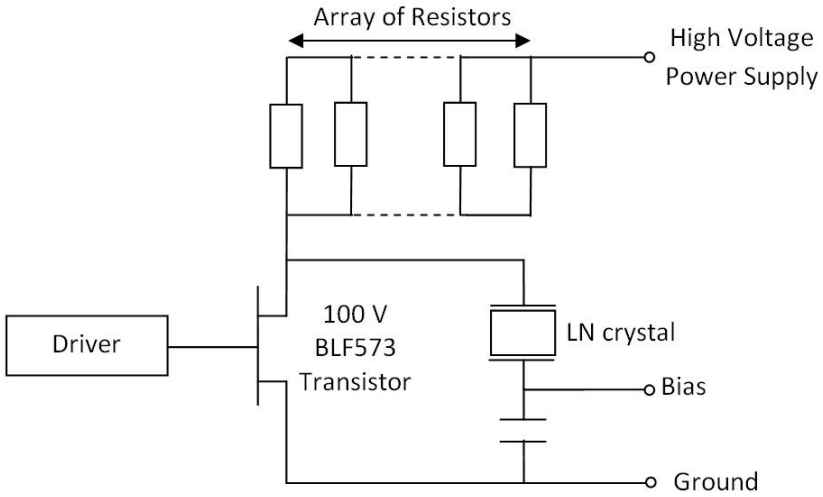

Figure 4.5: A simplified circuit diagram for light polarization switch using the LN crystal. When the circuit is switched on, the voltage from the power supply is applied to the crystal but no constant current is drawn. When the circuit is switched off (where power is not supplied to the crystal), the high power supply would be connected to the ground and a constant current is drawn. The switching on and off is done by the transistor controlled by an electrical signal.

paths - one to the crystal and the other to the ground. A 100 V BLF573 transistor was used to make the switch between these two paths. This switch is controlled by a driver circuit which is activated by a NIM signal. When there is no NIM signal to the driver, the high voltage power supply will be applying a voltage across the LN crystal. Since the LN crystal is effectively a capacitance, no huge constant current was drawn at this stage. When a NIM signal was sent to the driver, the high voltage power supply was connected to the ground. As such, a high current was passed through the circuit and the array of resistors would dissipate the electrical energy. A water chiller could be placed on top of the array of resistors to prevent the circuit board from overheating. The NIM signal was generated by a function generator and sent to a pulse shaper. The pulse shaper ensures that a negative NIM signal output has an approximately 300 pn fall and rise time. The bias voltage was used to operate the crystal at a negative voltage as well as to correct for any stray charges that are intrinsically stored in the LN crystal. In essence, during the switch off period, even though a high voltage is not supplied across crystal, it is still running through the circuit. The electrical power generated by the high voltage has to be dissipated. As such, if the voltages are too high, the electronic circuit might not be able to handle such a large power dissipation and cause the circuit to overheat. In addition, we require a low voltage transistor for a fast switch, as it is known that the response time of a transistor gets slower as the allowed voltage increases.

Since the half-wave voltage of the LN crystal was high, we went on to look at the behaviour of the output light at low voltages. From the theory of the Pockels effect, any voltages between 0 V to the crystal's half-wave voltage, the output light polarization is generally elliptical with an associated rotation in the plane of polarization in the major axis. If the losses due to the ellipticity are low, meaning that the visibility is still high while a rotation in the plane of polarization of the major axis is achieved, we are still able to use the LN for our fast polarization switch.

We designed with an experiment to investigate the plane of polarization rotation at low voltages as shown in figure 4.6. From the setup shown in figure 4.6, a horizontally polarized

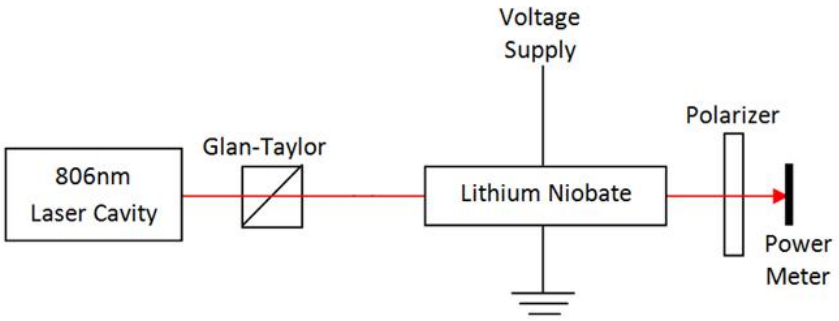

Figure 4.6: A schematic diagram of the setup to determine the angle of maximum intensity at various voltages applied through the LN crystal.

light was sent through the LN crystal. A polarizer was placed after the LN crystal so as to locate the plane of the polarization with the highest transmission intensity at the output. Unlike the determination of the half-wave voltage where the scanning of the voltage was started from 0 V, we looked at the behaviour of the output light from -50 V to 50 V. At each voltage, the polarizer was rotated until the highest intensity was registered by the power meter. The respective angular position on the polarizer was recorded.

After performing the experiment, the angular position of the maximum intensity of the output light against the voltage applied to the LN crystal is plotted in figure 4.7. It is seen from figure 4.7 that if a voltage of about (-39.16 ± 0.02) V was applied to the crystal, the angular position of the maximum intensity observed was at $(71 \pm 1)^\circ$. Furthermore, when a voltage of roughly (32.64 ± 0.02) V was applied, the angular position of the maximum intensity observed was at $(116 \pm 1)^\circ$. In other words, the plane of polarization at (-39.16 ± 0.02) V was rotated by 45° from the angular position of $(71 \pm 1)^\circ$ to that at $(116 \pm 1)^\circ$! If the plane of polarization of the light at angular position of $(71 \pm 1)^\circ$ is defined as the $|H\rangle$ polarization, the angular position of $(116 \pm 1)^\circ$ is therefore $|+\rangle$ polarization. Table 4.1 shows a summary

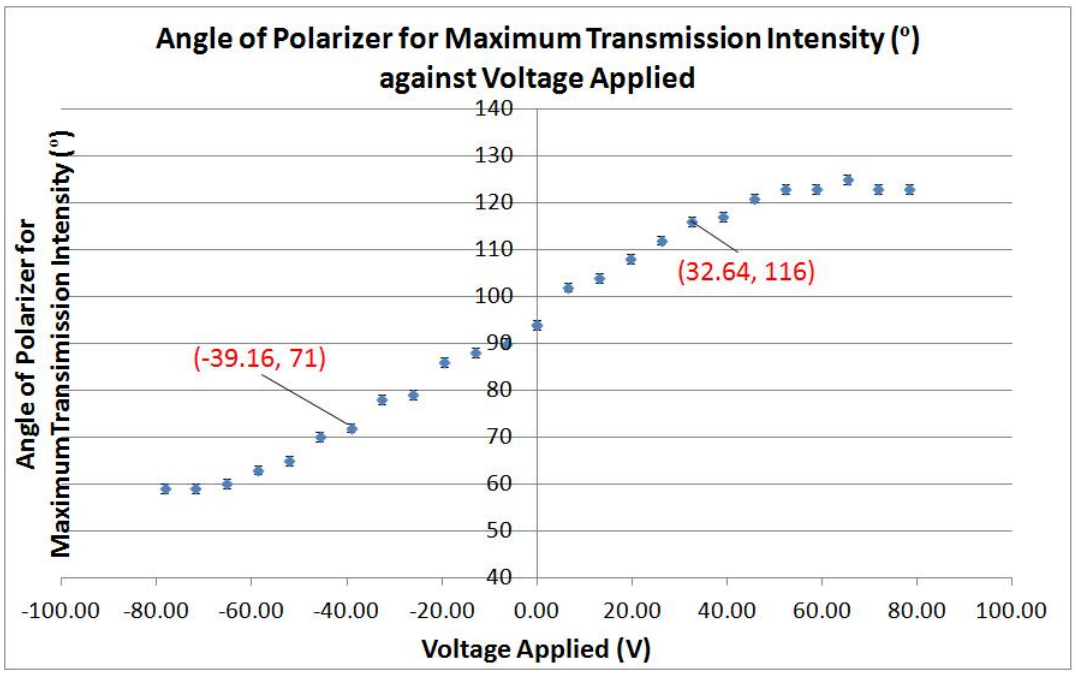

Figure 4.7: The plot of angle of polarizer(°) for maximum transmission intensity of the output light against voltage applied (V) across the crystal with H polarization as the input. This shows that a 45° rotation of the light polarization plane from 71° to 116° is possible at low voltages of (-39.16 ± 0.02) V and (32.64 ± 0.02) V respectively.

of the result that is consistent with our desired outcome as shown in table 2.1. We performed

Table 4.1: Summary of output polarization with different input polarization at new voltages that are lower.

	Output Polarization	
Input Polarization	Applied Voltage Across the Crystal	
	-39.16 V	32.64 V
$\|H\rangle$	$\|H\rangle$	$\|+\rangle$
$\|V\rangle$	$\|V\rangle$	$\|-\rangle$
$\|+\rangle$	$\|+\rangle$	$\|H\rangle$
$\|-\rangle$	$\|-\rangle$	$\|V\rangle$

the visibility measurement at the low applied voltage to the crystal. The result of the visibility against the voltage applied to the crystal is plotted as shown in figure 4.8. The plateau at high visibility in figure 4.8 tells us that we indeed can have a rotation of 45° while still maintaining high visibility with about 1% loss due to the linear polarized light becoming elliptical during the rotation at low voltages. As such, a rotation in the plane of polarization of the light and

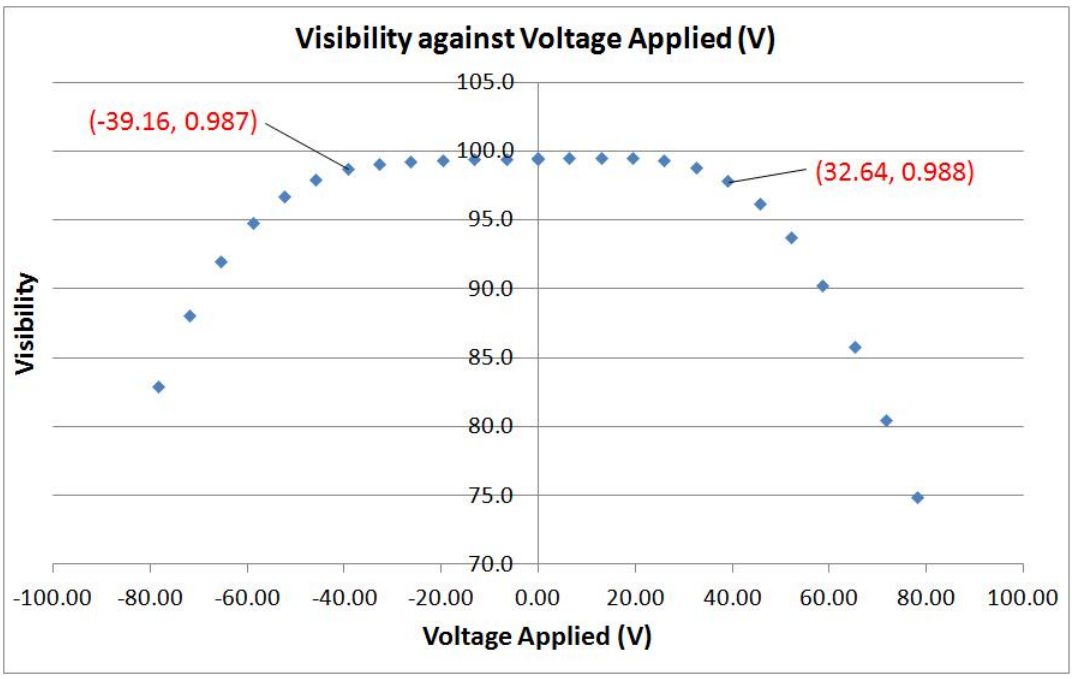

Figure 4.8: The visibility against voltage applied (V) across the crystal with H input polarization. The high visibility at low voltages shows that the output light polarization is relatively linear.

the change in the measurement bases are possible.

To investigate how the alignment of the crystal would affect the result, we misaligned the crystal slightly. We found out that the rotation now happened between (-6.5 ± 0.1) V and (58.8 ± 0.02) V as we switched from HV basis to $\pm 45°$ basis. This tells us that the switching voltages are not fixed for a particular alignment. This change in the switching voltages perhaps could be attributed to the effect of the crystal intrinsic birefringence effect as well as changing the path L through the crystal. The changing of the L is very sensitive as we are talking about interference of the e-ray and the o-ray of extremely short optical wavelength.

The main disadvantage of this sensitive alignment to the switching voltages is that for every alignment of the crystal, a characterization of the switching voltages and the respective visibilities must be done prior to any data acquisition process. This is because to get back the exact alignment that gives the same switching voltage is not a trivial task. The characterization step was hence always done prior to the investigation of the fast switching capability of the

crystal.

The discussion on the characterization of the LN crystal at an ultra slow (as compared to the 6 ns range) condition - where once the voltage is applied, the readings were taken after a few seconds - is complete and sufficient for the purpose of our project. We next investigate the effect of switching the voltage across the crystal at high frequency on the electro-optical crystal. Most importantly, the question is still are we able to rotate the polarization plane by 45°.

4.1.4 Investigating the Fast Switching Capability

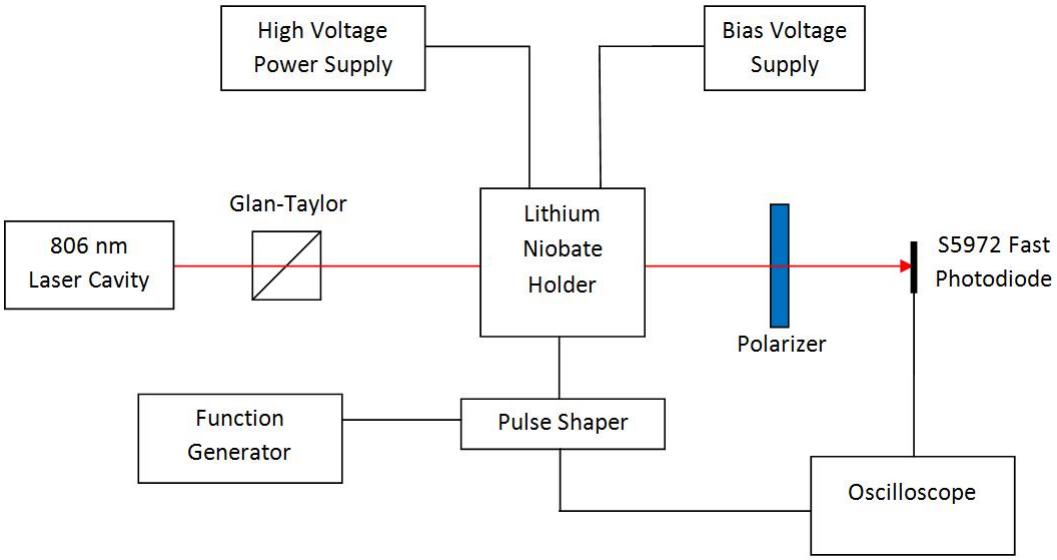

Figure 4.9: A schematic diagram of the setup to investigate the fast switching capability of the LN crystal.

Before we discuss the setup to investigate the fast switching response of the LN crystal, there are considerations that we have taken note in the design of the experimental setup. The LN crystal in the Pockels cell is like a capacitor and time is required for charges to accumulate on the gold plated electrode. Therefore, a high voltage power supply capable of supplying 6 A was used in this part of the experiment. In addition, this large power would have to be dissipated within nanoseconds range during the time in which the crystal is doing a switch. As such, it requires us to have an array of resistors capable of dissipating such a high power. The

experimental setup to test for the fast switching in the LN crystal is shown in figure 4.9. It is expected that there will be a large amount of heat generated and therefore a cooling method has to be included in the experiment setup which is not shown in figure 4.9.

A fast oscilloscope ($\sim$ 2 GHz) was used to monitor the NIM output signal from the pulse shaper as well as to measure the from the fast photodiode (Hamamatsu S5972 (at 500 MHz)). A simplified circuit diagram for photodetection using the high speed photodiode is shown in figure 4.10. The voltage of the fast photodiode is bias of about 12 V was sent into the circuit.

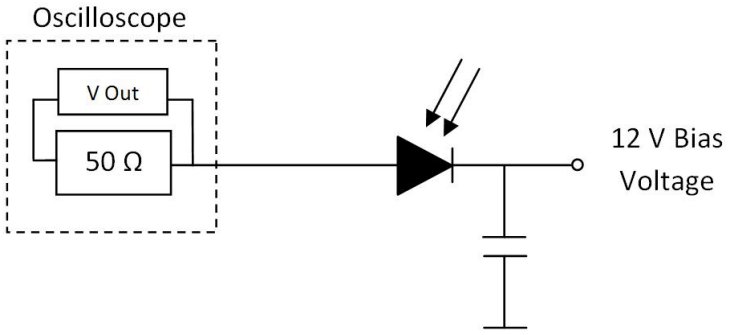

Figure 4.10: A simplified circuit diagram for the high speed Hamamatsu photodiode used to measure the fast optical response of LN crystal.

When the light was shone on the photodiode, a photocurrent was generated. The circuit was coupled to 50 Ω of the oscilloscope which would measure the fast response of the light intensity.

A new holder with the necessary electronics was constructed. Due to its larger size, we did not have the freedom of rotating the crystal with respect to a beam as described in section 3.3.3. Thus, for the alignment in this part of the experiment, a mirror was placed in front of the crystal so that there were enough degrees of freedom to walk the beam such that it was passed through the crystal properly. The alignment method is as follows. The crystal was placed roughly in the path of the laser beam. The laser beam was walked such that a nice circular beam profile observed with a camera on the other end of the crystal. A cross polarizer was placed before the crystal to minimize the intensity of the beam. Next, the crystal was removed and a pinhole was placed at a position after the crystal such that the beam was passed through

the pinhole. Thus, by placing the crystal back into the path of the laser beam (without the polarizer before the crystal), it was checked that the beam after the crystal did not deviate from the pinhole, ensuring that the beam has passed through the crystal in a straight path. The conoscopic interference pattern was also checked using the same method as mentioned in 3.3.3. Finally, fine adjustments were made such that the cross polarizer placed after the crystal registered a global minimum.

Table 4.2: A summary of the input light polarization on the left and the intensity at various output polarization at an applied voltage across the crystal of (-32.45 ± 0.02) V. A power meter was used to measure the intensity and the unit is in mW.

At Applied Voltage of -32.45 V	Output Polarization			
Input Polarization	$\|H\rangle$	$\|V\rangle$	$\|+\rangle$	$\|-\rangle$
$\|H\rangle$	2.758	0.01093	1.397	1.325
$\|V\rangle$	0.009662	2.744	1.385	1.430
$\|+\rangle$	1.453	1.300	2.692	0.06492
$\|-\rangle$	1.430	1.323	0.05964	2.700

Table 4.3: A summary of the input light polarization on the left and the intensity at various output polarization at an applied voltage across the crystal of (38.94 ± 0.02) V. A power meter was used to measure the intensity and the unit is in mW.

At Applied Voltage of 38.94 V	Output Polarization			
Input Polarization	$\|H\rangle$	$\|V\rangle$	$\|+\rangle$	$\|-\rangle$
$\|H\rangle$	1.414	1.330	2.736	0.01344
$\|V\rangle$	1.321	1.455	0.01205	2.750
$\|+\rangle$	2.729	0.03317	1.268	1.451
$\|-\rangle$	0.04998	2.723	1.518	1.248

We repeated the experiment mentioned in section 4.1.3 to find the switching voltage of the LN crystal in the new holder. We obtain a visibility of about (99 ± 1) % when H polarized light was passed through the crystal. The LN crystal was placed in between two copper slabs to minimise piezoelectric oscillations which will be discussed later. The voltages sent to the LN crystal were (-32.45 ± 0.02) V and (38.94 ± 0.02) V with the visibility high at (99 ± 1)%. Furthermore, we varied the input light polarization and measured the intensity output at various

polarizations at two switching voltages (-32.45 ± 0.02) V and (38.94 ± 0.02) V. The results are summarized in tables 4.2 and 4.3. The results in table 4.2 and 4.3 shows consistent results with the required rotation in the polarization planes as shown in table 4.1. Therefore. it shows that with a voltage step of about (71.4 ± 0.1) V, the rotations of the planes of polarization by 45° and the change in the measurement bases required in a Bell's inequality experiment is possible.

Next, we set the high voltage supply at about (71.4±0.1) V and the bias voltage at (−32.45± 0.02) V. In addition, as a start of this investigation, we would want to set a low duty cycle of the circuit. The duty cycle is the time proportion that the circuit is dissipating the electrical energy against the overall usage of the circuit. Thus, the function generator was used to set a pulse signal with a period of 100 ms and a pulse width of 20 μs that gives us a low duty cycle of about 0.0002 %. The height of the peak was set between -200 mV to -800 mV, as a negative pulse was required to generate a NIM pulse from the pulse shaper card. The polarizer was aligned parallel at the a voltage of (-32.45 ± 0.02) V was applied to the crystal. After switching on the NIM signal to our crystal holder, the result was obtained in figure 4.11. It can

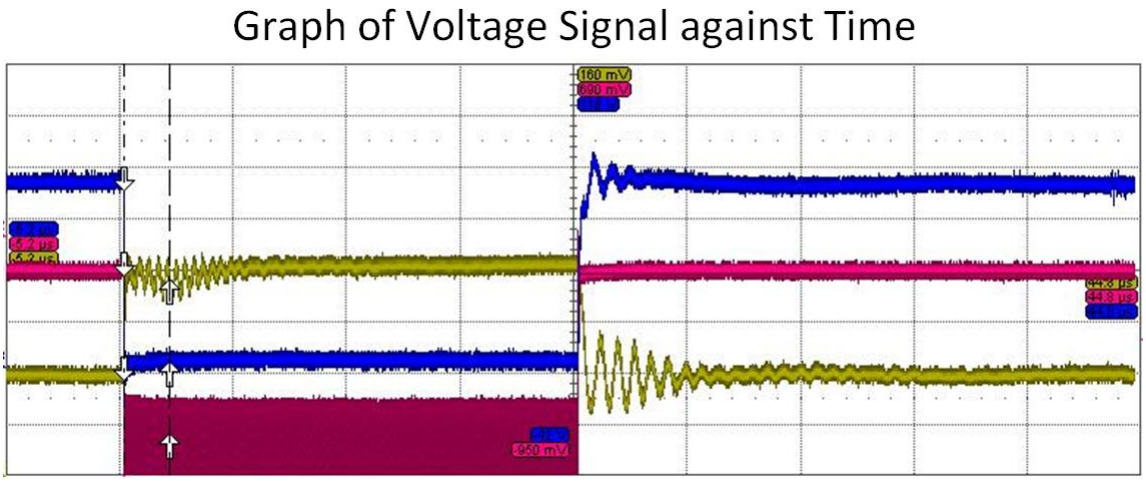

Figure 4.11: A clear piezoelectric ringing is seen in the optical response. Yellow trace shows the optical response: 20.0 mV/div. Blue trace shows the electrical response of the crystal: 20.0 mV/div. Red trace shows the electrical response of the crystal: 205 mV/div. The time scale was set at 5.00 μs/div.

be seen from figure 4.11 that there are oscillations in our optical responses instead of the ideal

flat plateau. The oscillations suggest that the output light from the crystals could be oscillating between two angles, or the light's polarization could be changing from less elliptical to more elliptical or a combination of the two effects as the LN crystal resonates. This is undesirable as they imply huge losses as their polarizations and the measurement bases are 'oscillating'. The loophole-free Bell's inequality experiment cannot afford such resonance effects.

The origin of such a resonance pattern could be termed as the piezoelectric ringing of the LN crystal. During the instance of switching off the voltages, due to the piezoelectric effect of the LN crystal, the distortion in the arrangement of atoms and electron clouds give rise to an oscillating change in the dimension of the crystal, especially in the direction where the voltage is applied. Since the birefringence effect is affected by the electric field across the crystal, which is in turn affected by the dimension of the crystal d, the optical response of the output light would oscillate as shown in figure 4.11. Using a simple model of explanation, the electric field across the crystal is given by

$$E = \frac{V}{d} \tag{4.12}$$

Taking the derivative with respect to the crystal thickness d that is changing significantly as compared to the other dimension,

$$\frac{\partial E}{\partial d} = -V\frac{1}{d^2} \tag{4.13}$$

$$\triangle E \approx -V\frac{1}{d^2}\triangle d \tag{4.14}$$

Since the birefringence is proportional to the applied electric field, and if d is oscillating, equation 4.14 tells us that the electric field across the crystal would oscillate as well, thus leading to the

oscillation in birefringence that affects the optical output response. Furthermore, the larger the voltage across the crystal, the larger the oscillations of the electric field. In addition, there is also effect due to the acousto-optical response of the LN crystal that might add on to the piezoelectric ringing, where the refractive index could change with the acoustic wave in the crystal. More understanding on this acousto-optical response is required and the simple model above did not take this into consideration.

From the traces in figure 4.11, the piezoelectric ringing dies off at about 5 μs at both the switching on and off of the high voltage power supply to the LN crystal. It is still considered long in terms of the nanosecond range that we wish to have for our switch. The amplitude of the piezoelectric ringing during the off period is smaller than that in the switching on period. This is consistent with the fact that the electrical response at the switching on period oscillates with larger amplitude that that of the switching off period. Hence, it implies that we might also reduce the effect of piezoelectric ringing by improving the LN crystal electronics circuit. More work in the future is required to investigate the effect on the piezoelectric ringing by varying the electrical components of the circuit.

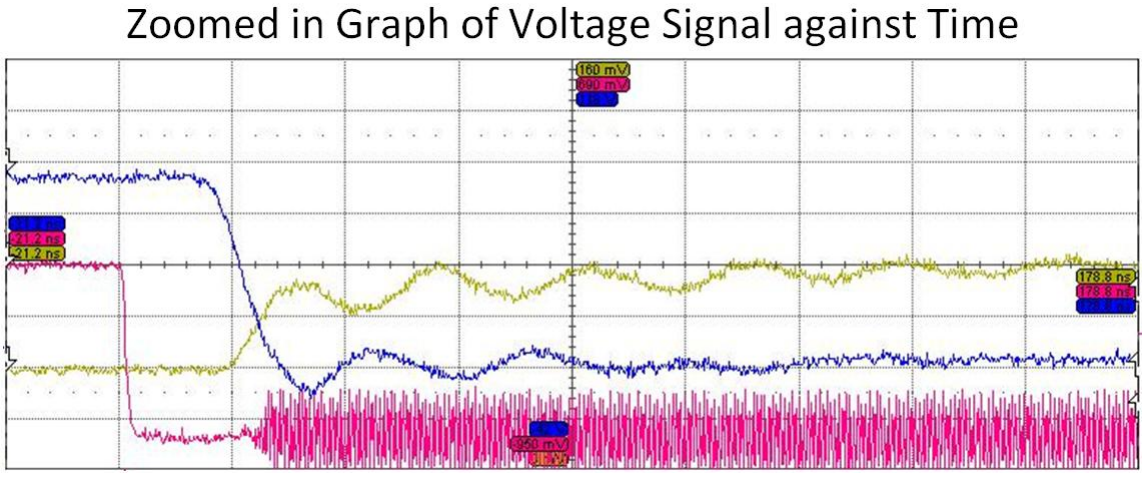

Figure 4.12: A zoomed in oscilloscope traces of the electrical signal, optical response and the trigger NIM signal at the switching off portion. The time scale here is zoomed in to 20.0 ns/div.

Lastly, to investigate the effectiveness of the circuit in switching, we zoomed in on the traces

to look at the response time of the electrical signal and the optical response of the LN crystal. The traces when the circuit is switched off are shown in figure 4.12. We see in figure 4.12 that the voltage across the crystal which is shown by the electrical signal (blue trace) takes about (14 ± 2) ns after the trigger switched off the circuit to start falling. The optical response would take a whole (20 ± 2) ns to start its discharging. The time constant for the electrical signal to fall to $\frac{3}{8}$ of the initial value is about (4 ± 2) ns and that for the rising of the optical signal to $\frac{5}{8}$ of the maximum value is about (6 ± 2) ns. Therefore, assuming that the problem of the piezoelectric ringing is solved, we know that in our circuit, we require a rise time of about (26 ± 4) ns for a complete swap from $|+\rangle$ basis to $|H\rangle$ basis using the LN crystal.

Chapter 5

On Going and Future Work

There are mainly three broad areas that we have to work on in the future. Firstly, we have to solve the piezoelectric ringing of the LN crystal. Secondly, we are currently work on closing the detection loophole. Finally, we would want to perform a loophole-free Bell's inequality experiment.

5.1 Minimzing the Piezoelectric Ringing

The results for the piezoelectric ringing in section 4.1.4 were obtained by placing the LN crystal in between two copper slabs with the hope of damping the oscillation in the optical response. The optical response before using the copper slabs is shown in figure 5.1. This shows that the oscillations persisted for a much longer time than when the copper slabs were used. This shows that we are in the right direction in resolving for the piezoelectric ringing effect. It is hoped that by encasing the LN crystal with other materials such as Manganese Oxide, which has similar acoustic impedance to the LN crystal, it can reduce the time in the damping of the oscillation. In addition, further investigation at a switching period of nanosecond range is to be done once

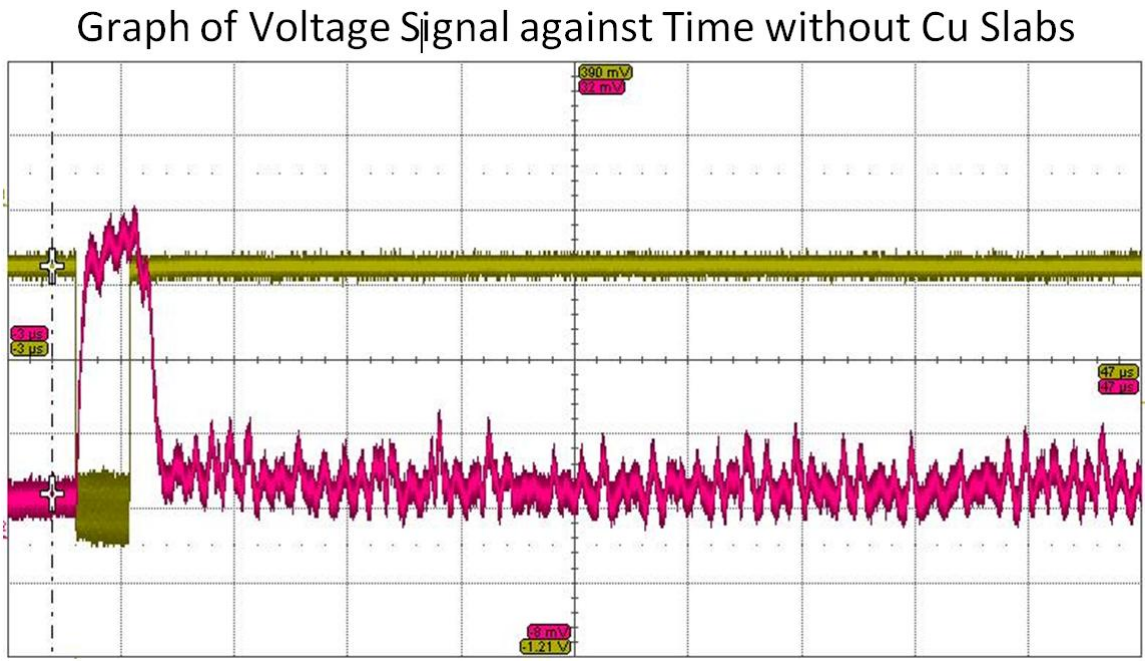

Figure 5.1: The piezoelectric ringing in the LN without the two copper slabs does not die out within 5 μs. The pink trace here is the optical response: 5.00 mV/div while the yellow trace is the NIM trigger: 200 mV/div. The time scale here is 5.00 μs/div.

the piezoelectric ringing issue is solved.

5.2 Closing the Detection Loophole - The Transition Edge Sensor

In the course of this project, we also work towards closing of the detection loophole concurrently. Nonetheless, due to various technical issues during the course of the project, we have to place this as an agenda in the near future. For closing of the detection loophole, we are working towards the detection efficiency limit of 66.6 % as shown by Eberhard [9]. Typical Silicon Avalanche Photodetectors (APDs) have low detection efficiency and thus, cannot be satisfactorily used to close the detection loophole. A new type of photodetector known as the Transition Edge Sensor (TES) would give us a detection efficiency of 99 % [12] and this seems promising in closing the detection loophole. The brief theory on how the TES works is as follows. The TES, which could

be made up of a Tungsten element is constantly cooled below its transition temperature where the tungsten is at its superconducting to normal transition state. The TES is then placed in a circuit as shown in figure 5.2. Before any photons shine on the TES, the bias voltage and

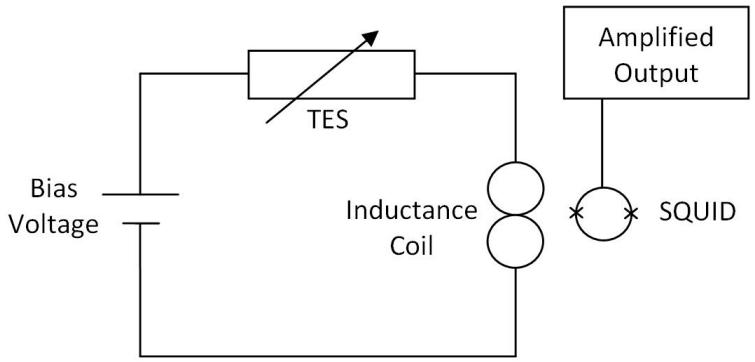

Figure 5.2: A simplified circuit of the TES. The changing magnetic field around the inductance coil due to the different number of photons impinging on the TES is measured by the Superconducting QUantum Interference Device - SQUID. The SQUID signal is amplified for display.

the resultant bias current create a bias power which the TES is heated up to and maintained at its transition temperature. After which, as photons hit on the TES, it absorbs the photons and gets heated up. As a result, the TES resistance increases further and causes a change in the current of the circuit. This change in the current would cause a change in the magnetic field in the vicinity of the inductance coil and gets picked up by the Superconducting QUantum Interference Device (SQUID), which is essentially a magnetometer. The output signal from the SQUID would give us a measurement on the amount of photons that impinge onto the TES. The circuit also self corrects itself to the transition temperature. Since the TES is constantly cooled, as its resistance increases, the bias power decreases and causes a decrease in the TESs' temperature back to its transition temperature. It is reported that such a method would give a detection efficiency of 99 % [12].

The cooling of the TES in this project was carried out in Graphene Research Laboratory led by Asst. Professor Ö. Barbaros while waiting for our own demagnetization refrigerator to come.

Work has been done on mounting the TES to a probe that will be inserted into the refrigerator for cooling. The pre-amplifier electronics to amplify the small signals from the SQUID and the necessary optical fibre in guiding the light to the TES have been completed. Up to the point of writing this thesis, our own demagnetization refrigerator has arrived. More work is required in the characterization of the TES for closing the detection loophole.

Finally, together with the photon pairs source that uses a Sagnac interferometer as shown in figure 5.3, we would want to perform a loophole-free Bell's inequality experiment eventually.

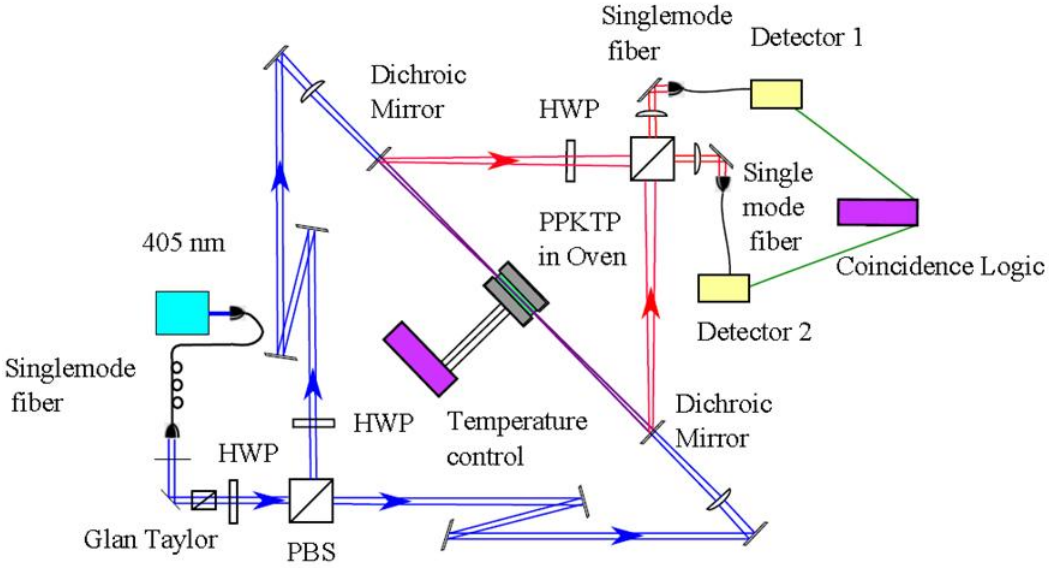

Figure 5.3: The overall experiment setup for the loophole-free Bell's inequality experiment. Note that the LN crystal and the TES are represented by the yellow box in this figure.

Chapter 6

Conclusion

There were several achievements accomplished in this project. The Pockels effect was observed in a LN crystal of dimension $1.5 \times 10 \times 100$ mm and its half-wave voltage at slow switching voltages was successfully determined to be approximately (150 ± 6) V. In addition, investigations show a rotation of the linear plane of polarization by 45° with reasonable visibility at a much lower voltage step about (71.4 ± 0.1) V. Different alignments would also cause the switching voltage to vary, therefore, a characterization of the voltages that allowed a rotation of 45° should be done after each alignment of the crystal before any meaningful data can be taken. Furthermore, we also found that the low frequency electro-optic coefficient r_{22} for a clamped LN crystal at 806 nm is experimentally determined to be about $(3.5 \pm 0.1) \times 10^{-12}$ mV^{-1} with the assumption from the Sellmeier equation that the o-ray refractive index of the LN crystal is (2.254 ± 0.002).

We also face a few challenges during the course of this project. The main challenge is the piezoelectric ringing of the LN crystal. Work must be done in the future to damp the oscillation as much as possible, or even remove the effect of such piezoelectric ringing. It is hoped that material with lower acoustic impedance like Manganese Oxide would help in

damping the peizoelectric ringing. The electrical response of our circuit gives us a minimum swapping time about (26 ± 4) ns, provided the problem with approximately 5 μs piezoelectric ringing is solved. The 5 μs piezoelectric ringing is still long as compared to the nanosecond time range that is required for our polarization switch. In addition, there are still more work to be done for the characterization of the TES for use in a Bell's inequality experiment, but preliminary results look promising.

In conclusion, the characterization of the LN crystal and the preliminary results from the TES in closing the detection loophole in this project suggest the possibility of eventually having a loophole-free Bell's inequality experiment and we are working in the right direction. It is only a matter of time before a convincing loophole-free Bell's inequality experiment is done and the race to be the first to accomplish it is perhaps the greatest motivation for the experimentalist in this field of research.

Reference

[1] J. F. Clauser and A. Shimony, *Bell's Theorem: Experimental Tests and Implications*, Rep. Prog. Phys, vol 41, pp. 1883-1927, 1978

[2] A. Einstein, B. Podolsky and N. Rosen, *Can Quantum-mechanics Description of Physical Reality be Considered Complete?*, Physical Review Letters, vol 47, pp. 777-780, 1935

[3] J. S. Bell, *On the Einstein Podolsky Rosen Paradox*, Physics 1, 195, 1964

[4] J. F. Clauser, M. A. Horne, A. Shimony and R. A. Holt, *Proposed Experiment to Test Local Hidden-Variable Theories*, Physical Review Letters, vol. 23, no. 15, pp. 880-884, 1969

[5] S. J. Freedman and J. F. Clauser, *Experimental Test of Local Hidden-Variable Theories*, Physical Review Letters, vol. 28, no. 14, pp. 938-941, 1972

[6] A. Aspect, J. Dalibard and G. Roger, *Experimental Test of Bell's Inequalities Using Time-Warying Analyzers*, Physical Review Letters, vol. 49, no. 25, pp. 1804-1807, 1982

[7] I. Gerhardt, Q. Liu, Antia Lamas-Linares, J. Skaar, V. Scarani, V. Makarov and C. Kurtsiefer, *Experimentally Faking the Violation of Bell's Inequalities*, Physical Review Letters, vol. 107, pp. 170404, 2011

[8] N. D. Mermin, *The EPR Experiment-Thoughts about "Loophole"*, Annals New York Academy of Sciences, pp. 422-427, 1985

[9] P. H. Eberhard, *Background Level and Counter Efficiencies Required for a Loophole-free Einstein-Podolsky-Rosen Experiment*, Physical Review A, vol. 47, no. 2, 1993

[10] M. A. Rowe, D. Kielpinski, V. Meyer, C. A. Sackett, W. M. Itano, C. Monroe and D. J. Wineland, *Experimental Violation of a Bell's Inequality with efficient detection*, Nature, vol. 409, pp. 791-794, 2001

[11] G. Weihs, T. Jennewein, C. Simon, H. Weinfurter and A. Zeilinger, *Violation of Bell's Inequality under Strict Einstein Locality Conditions*, Physical Review Letters, vol. 18, no. 23, pp. 5039-5043, 1998

[12] D. Rosenberg, A. E. Lita, A. J. Miller, S. W. Nam, *Noise-free, High-efficiency, Photon-number-Resolving Detectors*, Physical Review A, vol. 71, pp. 061803 2005

[13] D. C. Clary and B. J. Orr, *Optical, Electric and Magnetic Properties of Molecules - A Review of the Work of AD Buckingham*, Elsevier Science B.V. The Netherlands, 1997

[14] E. G. Sauter, *Nonlinear Optics*, USA: John Wiley & Sons, Inc, 1996

[15] L. Ricci, M. Weidemuller, T. Esslinger, A. Hemmerich, C. Zimmermann, V. Vuletic, W. Konig, T. T. Hansch, *A Compact Grating-Stabilized Diode Laser System for Atomic Physics*, Optics Communications, vol. 117, issues 5-6, pp. 541-549, 1995

[16] I. R. Kenyon, *The Light Fantastic - A Modern Introduction to Classical and Quantum Optics*, USA: Oxford University Press, 2008

[17] S. D. Smith, H. D. Riccius, R. P. Edwin, *Refractive Index of Lithium Niobate*, Optics Communications (Netherlands), vol. 17, pp. 332, 1976

[18] S. D. Smith, H. D. Riccius, R. P. Edwin, *Refractive Index of Lithium Niobate (errata)*, Optics Communications (Netherlands), vol. 20, pp. 188, 1977

[19] J. S. Bell, *Speakable and Unspeakable in Quantum Mechanics*, Cambride University Press, 1987

[20] C. C. Davis, *Lasers and Electro-Optics Fundamentals and Engineering*, United Kingdom, Cambridge: Cambridge University Press, 1996

Appendix A

Calculations

A.1 CHSH Bell's Inequality

A.1.1 State Invariant of Measurement Basis

We consider the state,

$$
\begin{aligned}
|\Psi_\alpha\rangle &= \frac{1}{\sqrt{2}}\left(|H_\alpha\rangle_1 \otimes |V_\alpha\rangle_2 - |V_\alpha\rangle_1 \otimes |H_\alpha\rangle_2\right) \\
&= \frac{1}{\sqrt{2}}[(-\sin\alpha|V\rangle_1 + \cos\alpha|H\langle_1)(\cos\alpha|V\rangle_2 + \sin\alpha|H\rangle_2) \\
&- (\cos\alpha|V\rangle_1 + \sin\alpha|H\rangle_1)(-\sin\alpha|V\rangle_2 + \cos\alpha|H\rangle_2)] \\
&= \frac{1}{\sqrt{2}}\left[(\sin^2\alpha + \cos^2\alpha)|H\rangle_1|V\rangle_2 + (-\sin^2\alpha - \cos^2\alpha)|V\rangle_1|H\rangle_2\right] \\
&= \frac{1}{\sqrt{2}}\left(|H\rangle_1 \otimes |V\rangle_2 - |V\rangle_1 \otimes |H\rangle_2\right) \qquad \text{(A.1)} \\
&= |\Psi^-\rangle \qquad \text{(A.2)}
\end{aligned}
$$

A.1.2 Probability Calculations

We present sample quantum mechanical calculations for the probabilities,

$$\begin{aligned} P(V,V|a,b) &= |\langle V_a|_1\langle V_b|_2|\Psi^-\rangle|^2 \\ &= |(\cos a\langle V|_1 + \sin a\langle H|_1)(\cos b\langle V|_2 + \sin b\langle H|_2)|\Psi^-\rangle|^2 \\ &= \frac{1}{2}(\sin a\cos b - \cos a\sin b)^2 \\ &= \frac{1}{2}\sin^2(a-b) \end{aligned} \tag{A.3}$$

$$\begin{aligned} P(H,V|a,b) &= |\langle H_a|_1\langle V_b|_2|\Psi^-\rangle|^2 \\ &= |(-\sin a\langle V|_1 + \cos a\langle H|_1)(\cos b\langle V|_2 + \sin b\langle H|_2)|\Psi^-\rangle|^2 \\ &= \frac{1}{2}(\sin a\sin b + \cos a\cos b)^2 \\ &= \frac{1}{2}\cos^2(a-b) \end{aligned} \tag{A.4}$$

which are shown in equations 2.6.

A.1.3 Derivation

The derivation of the CHSH inequality shown in equation 2.5 is inspired from the Appendix 2 of chapter 16 - *Bertlmann's Socks and the Nature of Reality* found in [19]. Starting from equation 2.4, the expectation value for settings a and b is given by,

$$E(a,b) = P(+1,+1|a,b) + P(-1,-1|a,b) - P(+1,-1|a,b) - P(-1,+1|a,b) \tag{A.5}$$

$$= \int f(\lambda)\left[P_1\left(+1|a,\lambda\right) - P_1\left(-1|a,\lambda\right)\right]\left[P_2\left(+1|a,\lambda\right) - P_2\left(-1|a,\lambda\right)\right]\,\mathrm{d}\lambda \tag{A.6}$$

$$= \int f(\lambda)\bar{A}(a,\lambda)\bar{B}(b,\lambda)\,\mathrm{d}\lambda \tag{A.7}$$

where $\bar{A}$ and $\bar{B}$ represent the first and the second brackets respectively. The integral is taken over all values of the hidden variables, and $f(\lambda)$ is the appropriate probability distribution for λ. Since the probability Ps are always between 0 and 1,

$$|\bar{A}(a,\lambda)| \leq 1 \text{ and } |\bar{B}(b,\lambda)| \leq 1 \tag{A.8}$$

Now we consider the addition of the expectation values such as,

$$\begin{aligned} E(a,b) \pm E(a,b') &= \int \left[\left(f(\lambda)\bar{A}(a,\lambda)\bar{B}(b,\lambda)\right) \pm \left(f(\lambda)\bar{A}(a,\lambda)\bar{B}(b',\lambda)\right)\right] \mathrm{d}\lambda \qquad \text{(A.9)} \\ &= \int f(\lambda)\bar{A}(a,\lambda)\left[\bar{B}(b,\lambda) \pm \bar{B}(b',\lambda\right] \mathrm{d}\lambda \qquad \text{(A.10)} \end{aligned}$$

From equation A.8, it follows that,

$$|E(a,b) \pm E(a,b')| \leq \int f(\lambda)\left[\bar{B}(b,\lambda) \pm \bar{B}(b',\lambda\right] \mathrm{d}\lambda \tag{A.11}$$

Similarly,

$$|E(a',b) \mp E(a',b')| \leq \int f(\lambda)\left[\bar{B}(b,\lambda) \mp \bar{B}(b',\lambda)\right] \mathrm{d}\lambda \tag{A.12}$$

Again, from equation A.8,

$$|\bar{B}(b,\lambda) \pm \bar{B}(b',\lambda)| + |\bar{B}(b,\lambda) \mp \bar{B}(b',\lambda)| \leq 2 \tag{A.13}$$

Like all probability distribution, $f(\lambda)$ is non negative and must satisfy the normalization condition,

$$\int f(\lambda)\,\mathrm{d}\lambda = 1 \tag{A.14}$$

Therefore, it follows that,

$$|E(a,b) \pm E(a,b')| + |E(a',b) \mp E(a',b')| \leq 2 \tag{A.15}$$

which is included in equation 2.5.

A.2 Working of a Half-Wave Plate

The π phase difference between the e-ray and the o-ray is a property that we intend to use for our Pockels cell when the half-wave voltage applied to it. To see how the π phase difference changes our output light after passing through the crystal, let us first look at the matrix representation of an anticlockwise rotation of the light in a HV basis by an angle of Θ, which is given by

$$T = \begin{pmatrix} \cos\Theta & \sin\Theta \\ -\sin\Theta & \cos\Theta \end{pmatrix} \tag{A.16}$$

Keeping equation A.16 in mind, we look at the axes of the orthogonal polarizations of the e-ray and the o-ray, which could be labelled as the $\hat{F}$ and $\hat{S}$ axes respectively. In practical situations, the $\hat{F}$ and $\hat{S}$ axes of the crystal can be rotated with respect to the linearly polarized light. If we choose a HV basis to describe the linear polarization of the light, the $\hat{F}$ and $\hat{S}$ axes could be rotated anticlockwise with respect to the HV basis as shown in figure A.1. As such, we could write the transformation equation in the form of,

$$\begin{pmatrix} \hat{F} \\ \hat{S} \end{pmatrix} = \begin{pmatrix} \cos\theta & \sin\theta \\ -\sin\theta & \cos\theta \end{pmatrix} \cdot \begin{pmatrix} \hat{H} \\ \hat{V} \end{pmatrix} \tag{A.17}$$

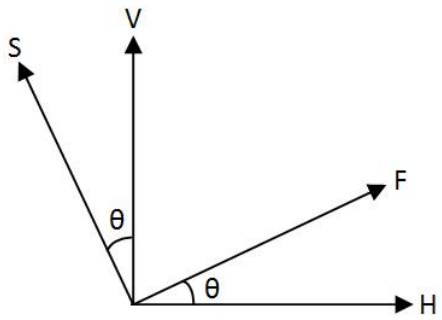

Figure A.1: The anticlockwise rotation of the $\hat{F}$ and $\hat{S}$ axes by an angle θ from the original HV basis.

and the clockwise rotation from the HV basis to the $\hat{F}$ and $\hat{S}$ axes is,

$$\begin{pmatrix} \hat{H} \\ \hat{V} \end{pmatrix} = \begin{pmatrix} \cos\theta & -\sin\theta \\ \sin\theta & \cos\theta \end{pmatrix} \cdot \begin{pmatrix} \hat{F} \\ e^{i\phi}\hat{S} \end{pmatrix} \tag{A.18}$$

Since we are interested in the phase difference between the $\hat{F}$ and $\hat{S}$ axes, we consider the $\hat{S}$ is the only ray that is retarded with respect to $\hat{F}$, such that $\hat{S} \rightarrow e^{i\phi}\hat{S}$ while $\hat{F} \rightarrow \hat{F}$, where $e^{i\phi}$ describes a retardation by ϕ. When the phase difference is π, $e^{i\pi} = -1$. Combining this fact with equations A.17 and A.18, it can be shown that

$$\begin{pmatrix} \hat{H} \\ \hat{V} \end{pmatrix} = \begin{pmatrix} \cos 2\theta & \sin 2\theta \\ -\sin 2\theta & \cos 2\theta \end{pmatrix} \cdot \begin{pmatrix} \hat{H} \\ \hat{V} \end{pmatrix} \tag{A.19}$$

Now, comparing the transformation matrix in equation A.19 with the anticlockwise rotation matrix in equation A.16, it essentially tells us that as the linearly polarized light passed through the crystal at an angle θ with respect to the $\hat{F}$ axis, the plane of polarization of the output light will be rotated by 2θ with respect to the input light. The transformation matrix,

$$T' = \begin{pmatrix} \cos 2\theta & \sin 2\theta \\ -\sin 2\theta & \cos 2\theta \end{pmatrix} \tag{A.20}$$

is also known as the *Jones matrix* of the optical element known as the half-wave plate (HWP) which is used to rotate linear polarization of light.

A.3 Mathematics of Pockels Effect

The mathematics for the Pockles effect can be found in more details in [14]. We will discuss the important steps in the mathematical treatment in a concise manner that leads to a conclusion of the linear proportionality of a birefringence with an applied electric field. The magnitude of refractive indices and their respective orientations in the crystal can be described by the mathematics diagram known as the index ellipsoid. The index ellipsoid equation of an optically uniaxial medium is given by,

$$1 = \sum_{i=0}^{3} \frac{x_i^2}{n_{x_i}^2} = (x_1, x_2, x_3) \cdot \begin{bmatrix} \frac{1}{n_{x_1}^2} & 0 & 0 \\ 0 & \frac{1}{n_{x_2}^2} & 0 \\ 0 & 0 & \frac{1}{n_{x_3}^2} \end{bmatrix} \cdot \begin{bmatrix} x_1 \\ x_2 \\ x_3 \end{bmatrix} \tag{A.21}$$

where x_1, x_2 and x_3 are the principal axes of the crystal and n_{x_1}, n_{x_2} and n_{x_3} are the principal refractive indices in the x_1, x_2 and x_3 directions respectively. The refractive indices have to fit the description of equation A.21 when there is no applied electric field. As we turn on an applied DC electric field that is directed along the principal axes of the crystal, the index ellipsoid is,

$$1 = \sum_{i=0}^{3} \frac{x_i^2}{n_{x_i}^2} + \left(x_1^2, x_2^2, x_3^2, 2x_2x_3, 2x_1x_3, 2x_1x_2\right) \cdot \begin{bmatrix} r_{11} & r_{12} & r_{13} \\ r_{21} & r_{22} & r_{23} \\ r_{31} & r_{32} & r_{33} \\ r_{41} & r_{42} & r_{43} \\ r_{51} & r_{52} & r_{53} \\ r_{61} & r_{62} & r_{63} \end{bmatrix} \cdot \begin{bmatrix} \hat{E}_1 \\ \hat{E}_2 \\ \hat{E}_3 \end{bmatrix} \tag{A.22}$$

where r_{ij} are the electro-optic coefficients of the crystal and the 6×3 matrix of the electro-optic coefficients is often known as the electro-optic tensor. More than often, the symmetry considerations vanish some of the 18 elements of r_{ij}. For the LN crystal in this project, its electro-optic tensor is,

$$\bar{r} = \begin{bmatrix} 0 & -r_{22} & r_{13} \\ 0 & r_{22} & r_{13} \\ 0 & 0 & r_{33} \\ 0 & r_{51} & 0 \\ r_{51} & 0 & 0 \\ -r_{22} & 0 & 0 \end{bmatrix} \tag{A.23}$$

With that, equation A.22 becomes,

$$\left(\frac{1}{n_{x_1}^2} - r_{22}E_2\right)x_1^2 + \left(\frac{1}{n_{x_2}^2} + r_{22}E_2\right)x_2^2 + \frac{x_3^2}{n_{x_3}^2} + 2r_{51}E_{x_2}x_2x_3 = 1 \tag{A.24}$$

From equation A.24, we can see that if there is no applied electric field to the crystal, equation A.24 neatly collapses into equation A.21. This is consistent with the physical observation of the electro-optic effect. It is also intuitively logical that if we are able to write equation A.24 in the same form as the index ellipsoid in equation A.21, meaning,

$$1 = \sum_{i=0}^{3} \frac{x_i'^2}{n_{x_i}'^2} = \frac{x_1'^2}{n_{x_1}'^2} + \frac{x_2'^2}{n_{x_2}'^2} + \frac{x_3'^2}{n_{x_3}'^2} \tag{A.25}$$

we would be able to find the new principal axes x_i' and new refractive indices n_{x_i}' along the new axes due to the effect of the applied electric field. The rigour mathematics in getting equation A.24 has been done in [20]. Applying the static DC electric field along the x_2 axis of the crystal,

it gives the following results to the first order approximation,

$$n^{'}_{x^{'}_1} = n_o + \frac{1}{2} n_o^3 r_{22} E_2 \tag{A.26}$$

$$n^{'}_{x^{'}_2} = n_o - \frac{1}{2} n_o^3 r_{22} E_2 \tag{A.27}$$

$$n^{'}_{x^{'}_3} = n_e \tag{A.28}$$

where the new $x^{'}_1$ and $x^{'}_2$ axes are approximately no change with the initial x_1 and x_2 axis. The new refractive indices allow us to calculate the birefringence due the applied electric field,

$$\left(n^{'}_{x^{'}_1} - n^{'}_{x^{'}_2} \right) = \Delta n = n_o^3 r_{22} E_2 \tag{A.29}$$

which exactly shows the Pockels effect where the birefringence is proportional to the applied electric field. The phase difference Γ between the e-ray and the o-ray would then be defined as,

$$\Gamma = \frac{2\pi}{\lambda} \Delta n L = \frac{2\pi}{\lambda} n_o^3 r_{22} E_2 L \tag{A.30}$$

$$\Gamma = \pi \cdot \frac{V}{V_\pi} \tag{A.31}$$

with the so-called half-wave voltage,

$$V_\pi = \frac{\lambda}{2 n_o^3 r_{22}} \cdot \frac{d}{L} \tag{A.32}$$

where V is the applied voltage across the crystal with thickness d and L is the length of the crystal along the propagation of the light.

A.4 Analyzer Intensity Dependency on Phase Difference

The electric field of the light after the first polarizer at $+45^\circ$ is,

$$\begin{aligned}\hat{E} &= E_0 \cos(\omega t)\hat{a} \\ &= \frac{1}{\sqrt{2}}\cos\omega t\left[\frac{1}{\sqrt{2}}(\hat{a}+\hat{b})\right] + \frac{1}{\sqrt{2}}\cos\omega t\left[\frac{1}{\sqrt{2}}(-\hat{a}+\hat{b})\right] \end{aligned} \tag{A.33}$$

where E_0 is the amplitude of the electric field, ω is the frequency of the light and $\hat{a}$ and $\hat{b}$ is the unit vectors in the $+45^\circ$ and -45° directions respectively. It is to note that $\frac{1}{\sqrt{2}}(\hat{a}+\hat{b})$ and $\frac{1}{\sqrt{2}}(-\hat{a}+\hat{b})$ are the $\hat{x}$ and $\hat{y}$ of the principle axes of the crystal respectively. After passing through the LN crystal, the light wave would be,

$$\hat{E}_2 = \frac{1}{\sqrt{2}}E_0\cos(\omega t+\Gamma)\hat{x} + \frac{1}{\sqrt{2}}E_0\cos(\omega t)\hat{y} \tag{A.34}$$

where it can be said that the light with its electric field oscillating parallel to the x axis is retarded while the the light with its electric field oscillating parallel to the y is not retarded. The polarizer after the crystal is placed parallel to the $\hat{b}$ direction. Therefore, the electric field after the polarizer is given as,

$$\begin{aligned}\hat{E}_3 &= (\hat{E}_2\cdot\hat{b})\hat{b} \\ &= \left[\frac{1}{\sqrt{2}}E_0\cos(\omega t+\Gamma)\hat{x}\cdot\hat{b} + \frac{1}{\sqrt{2}}E_0\cos\omega t\hat{y}\cdot\hat{b}\right]\hat{b} \\ &= \frac{1}{2}E_0[\cos(\omega t+\Gamma)-\cos\omega t]\hat{b} \\ &= -E_0\sin\frac{\Delta\Gamma}{2}\sin\left[\omega t+\frac{\Gamma}{2}\right] \end{aligned} \tag{A.35}$$

The intensity is directly proportional to the electric field of the light. Therefore, the intensity after the polarizer is given by,

$$\begin{aligned} I &= |-E_0 \sin\frac{\Gamma}{2}|^2 \\ &= E_0^2 \sin^2\frac{\Gamma}{2} \\ &= I_0 \sin^2\frac{\Gamma}{2} \end{aligned} \tag{A.36}$$

which is shown in equation 4.2.

Appendix B

Alignment Steps for Lithium Niobate

B.1 Alignment With x and y Rotation Crystal Holder

Figure B.1: Step 1: Ensure that the light is collimated through C230 TME B Lens of about 4.0 mm focal length. Light is H polarized here.

Figure B.2: Step 2: Place 2 pinholes of equal height in. Ensure the light passes through both pinholes. In the diagrams under this section, filled pinhole means that the pinhole is closed, clear means otherwise.

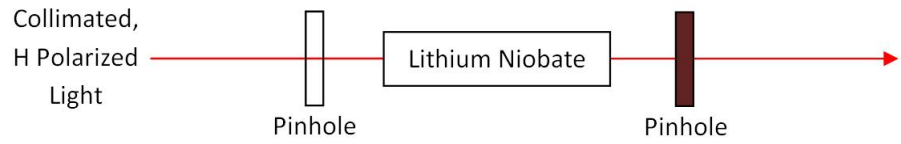

Figure B.3: Step 3: Insert the crystal, ensure that the light still passes through the pinhole after the crystal, thus the light beam is not bent while passing through the crystal.

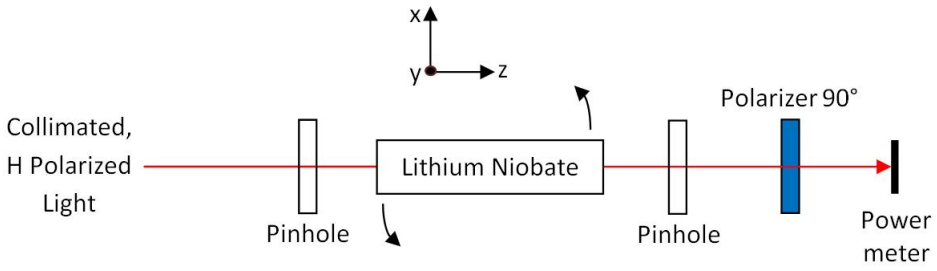

Figure B.4: Step 4: Place a crossed polarizer and the power meter. Look for a global minimum by rotating the crystal about the y axis.

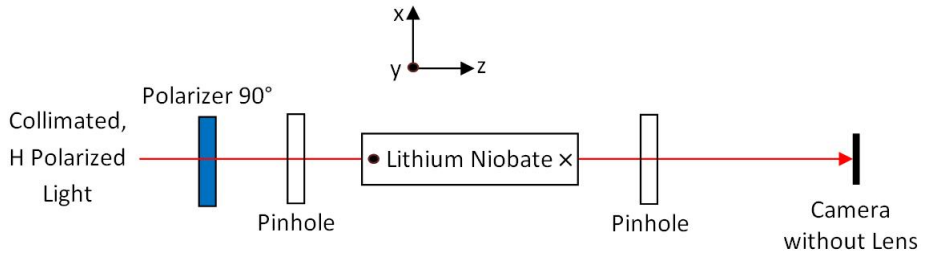

Figure B.5: Step 5: Shift the polarizer before the crystal, replace the power meter with a camera, without its lens. Look for a circular beam profile by rotating the crystal about the x axis.

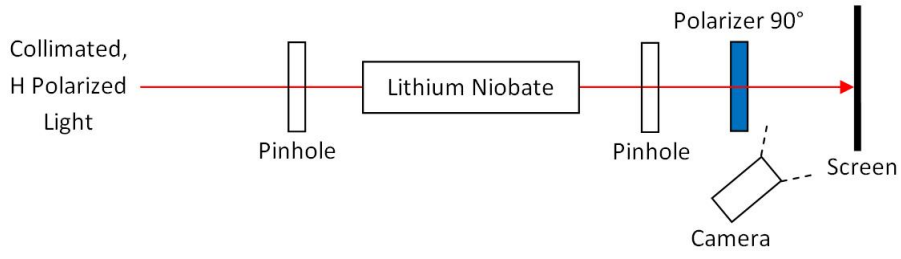

Figure B.6: Step 6: Shift the polarizer back to the position after the crystal, stick a cellulose tape in front of the crystal holder. Place a screen to capture the output image and look for the conoscopic interference pattern through the camera with the lens.

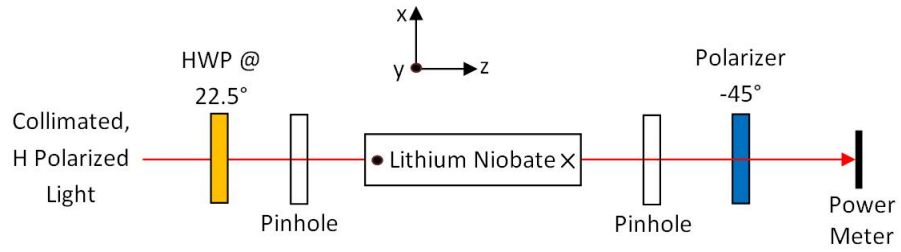

Figure B.7: Step 7: Insert a hwp at 22.5° and the polarizer at 45°. Perform fine rotation in the x axis to obtain a global minimum intensity after the polarizer.

B.2 Alignment Without x and y Rotation Crystal Holder

Figure B.8: Step 1: Ensure that the light is collimated through C230 TME B Lens of about 4.0 mm focal length. Light is H polarized here.

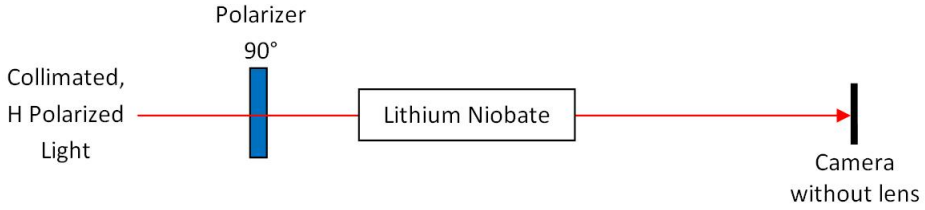

Figure B.9: Step 2: Insert polarizer at 90°, crossed polarizer with the H polarized light. Place in the crystal and camera without lens to get a nice circular beam profile.

Figure B.10: Step 3: Remove crystal and place in a pinhole. Ensure that the light passes through the pinhole.

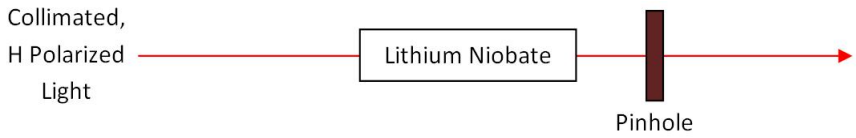

Figure B.11: Step 4: Place back the crystal. Ensure that the light still passes through the pinhole.

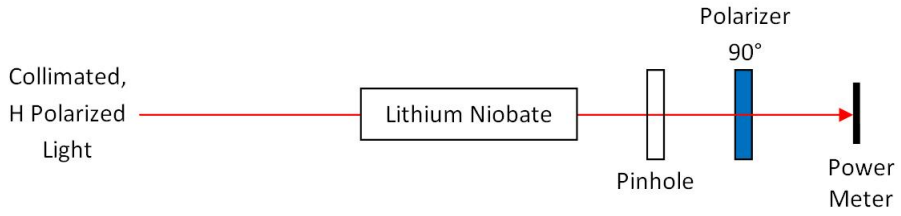

Figure B.12: Step 5: Insert a polarizer at 90° and walk the bottom screw of the mirror mount to obtain a global minimum intensity after the polarizer.

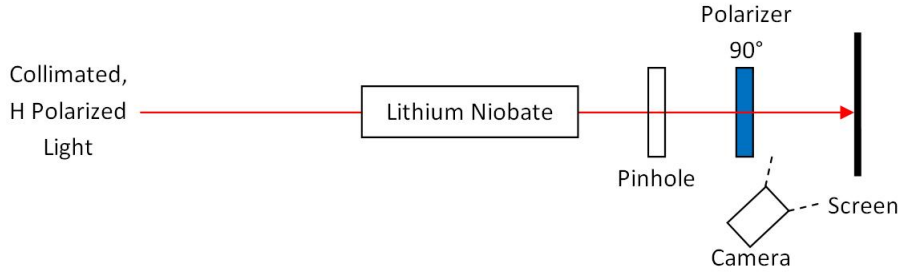

Figure B.13: Step 6: Replace the power meter with a screen and check for conoscopic interference pattern by sticking a cellulose tape in front of the LN crystal.

Appendix C

Error Analysis

C.1 Visibility Calculations

From the visibility graph obtained in figure 3.5, we plot a curve fit with the function,

$$f(x) = a \sin\left(\frac{2\pi}{180}x\right) + b \cos\left(\frac{2\pi}{180}x\right) + c \tag{C.1}$$

where a, b and c are the fitting parameters and x is the polarizer angle. The curve fit using the SciDAVis programme is shown in figure C.1. The R^2 of the fit is 0.991 and the values generated for the fitting parameters are,

$$a = 0.853 \pm 0.012,\ b = -1.450 \pm 0.012 \text{ and } c = 2.146 \pm 0.0085 \tag{C.2}$$

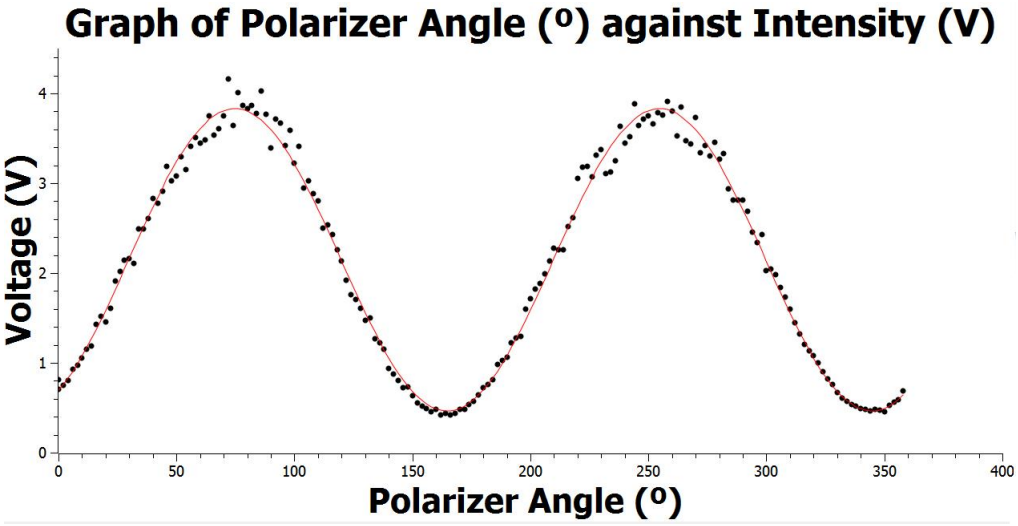

Figure C.1: The visibility curve fit used to calculate the visibility and its error.

Defining,

$$A1 = \sqrt{a^2 + b^2} \tag{C.3}$$

$$\Delta A1 = \frac{a}{a^2 + b^2}\Delta a + \frac{b}{a^2 + b^2}\Delta b \tag{C.4}$$

$$I_{max} = A1 + c \tag{C.5}$$

$$I_{min} = -A1 + c \tag{C.6}$$

$$\Delta I_{max} = \Delta I_{min} \tag{C.7}$$

$$= \Delta A1 + \Delta c \tag{C.8}$$

The visibility is then calculated using equation 3.1 is given to be 78.4 %, with uncertainty,

$$\Delta\text{Visibility} = \frac{\partial\text{Visibility}}{\partial I_{max}}\Delta I_{max} + \frac{\partial\text{Visibility}}{\partial I_{min}}\Delta I_{min} \tag{C.9}$$

$$= \left[\frac{1}{I_{max} + I_{min}} - \frac{I_{max} - I_{min}}{(I_{max} + I_{min})^2}\right]\Delta I_{max} \tag{C.10}$$

$$- \left[\frac{1}{I_{max} + I_{min}} + \frac{I_{max} - I_{min}}{(I_{max} + I_{min})^2}\right]\Delta I_{min} \tag{C.11}$$

$$\approx 0.004 \tag{C.12}$$

C.2 High Voltage Card

Arbitrary inputs to a computer programme control the actual voltage applied across the crystal. Therefore, characterization of the high voltage card of actual voltage outputs against the arbitrary inputs is done and shown in figure C.2. The voltage output was measured using a Digital Multimeter (DMM). The calibration curve was used to determine the voltage applied

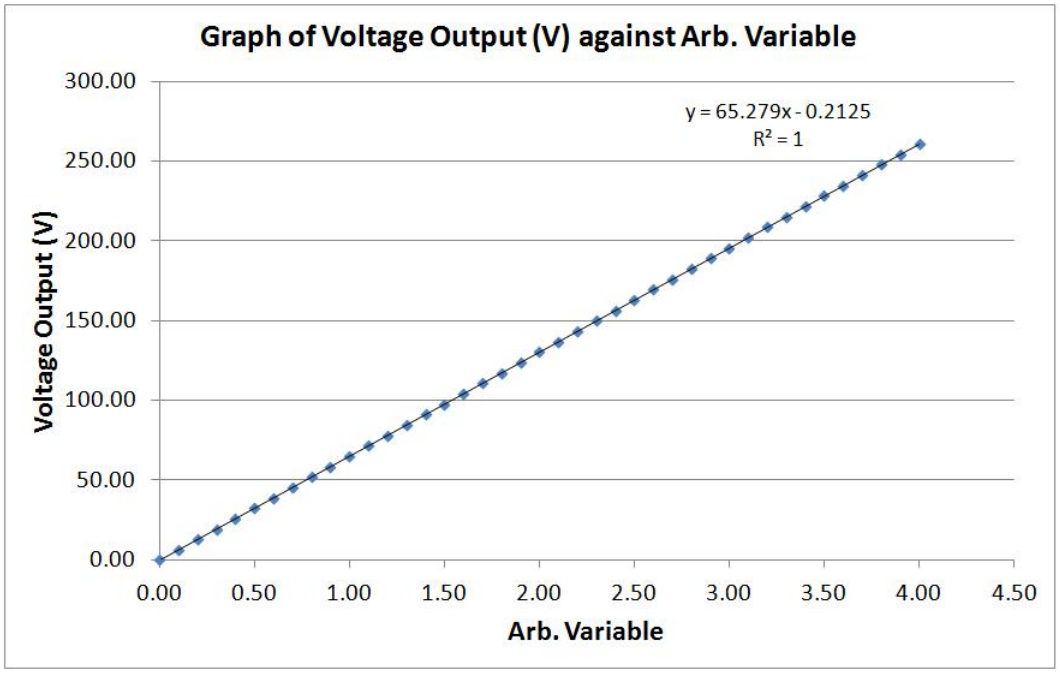

Figure C.2: Graph of actual voltage outputs against the arbitrary inputs. The fluctuations was not observed in the DMM, thus the error bar is taken to be ±0.1 V which is too small to be shown on the graph.

to the crystal in various the investigations. The minimum uncertainty in the voltage value ΔV is given to be,

$$\Delta V = \frac{\Delta m}{m} \times x + \Delta c \tag{C.13}$$

where m and c are the gradient and vertical axis intercept. Δm and Δc are the standard deviations of the gradient and the intercept obtained from the graph. x is the arbitrary inputs.

C.3 Error bars

C.3.1 Half-Wave Voltage Graph

The horizontal error bars for the graph in figure 4.3 that gives us the half-wave voltage is given (as well as that for the linear graph in figure 4.4 for determining the r_{22} and for the graph in figure 4.7) by equation C.13. Showing a sample calculation to illustrate the magnitude of the error bar at half-wave voltage,

$$\Delta V = 65.279 \times 2.3\frac{0.007}{65.279} + 0.017 \approx 0.034\text{V} \tag{C.14}$$

The vertical error bar for the graph in figure 4.3 that gives us the half-wave voltage is given by,

$$\Delta\left(\frac{I}{I_0}\right) = \frac{I}{I_0}\sqrt{\left(\frac{\Delta I}{I_0}\right)^2 + \left(\frac{\Delta I}{I}\right)^2} \tag{C.15}$$

where ΔI is the intensity fluctuations observed from the power meter. As the external laser cavity produce a laser beam with power stability, occasional power fluctuation is at 0.05 V, even though most of the time it was observed that the power fluctuation is within 0.02 V. Thus $\Delta I = \pm 0.05$ V Using the data at the half-wave voltage to exemplify the order of the error bar,

$$\Delta\left(\frac{I}{I_0}\right) = 3.18\sqrt{\left(\frac{0.05}{8.43}\right)^2 + \left(\frac{0.05}{8.41}\right)^2} \approx \pm 0.0084 \tag{C.16}$$

Both error bars are too small to be shown on the graph. This is especially so for the horizontal error bars for all graphs in this project.

C.3.2 r_{22} Linear Graph

Let y the normalized intensity $\frac{I}{I_0}$. Since $\Gamma = 2\sin\sqrt{\frac{I}{I_0}}$, the vertical error bars for the linear graph in figure 4.4 to determine the r_{22} is given by,

$$\Delta\Gamma = 2\left.\frac{\partial(\sin\sqrt{y})}{\partial y}\right|_y \Delta y = \frac{2}{\sqrt{y-y^2}}\Delta y \tag{C.17}$$

Using the half-wave voltage as an example,

$$\Delta\Gamma = \frac{2}{\sqrt{0.998-0.998^2}} \times 0.0084 \approx \pm 0.34 \text{ rad} \tag{C.18}$$

C.4 Curve Fitting

The r^2 value and the χ^2 value for the graph used to determine the half-wave voltage are determined to compare the experimental results with the theoretical fit as shown in figure 4.3 from 6.315 V to the half-wave voltage. The analysis excludes the possible Kerr effect at higher voltage. Using the SciDAVis software, the r^2 value is given to be 0.9892. The χ^2 values is calculated from,

$$\chi^2 = \sum_{i=1} \frac{y_e - y_t}{y_t} = 0.09692 \tag{C.19}$$

Using the χ^2 distribution table with 23 degrees of freedom (23 data points), the χ^2 value at 95 % confidence is 35.17. Since the experimental $\chi^2 = 0.09692$ which is smaller than 35.17, the experimental trend is consistent with the theoretical trend within 95% confidence interval.

C.5 Uncertainty in $n_o^3 r_{22}$ Determination

The bandwidth of the laser beam from the external laser cavity is around 50 fm. The uncertainty in the refractive index Δn_o using the Sellmeier equation is (assuming no error in the determination of the Sellmeier constants),

$$\begin{aligned} \Delta n_o &= \frac{\partial n_o}{\partial \lambda}\Delta\lambda \\ &= \frac{\frac{2B\lambda}{(\lambda^2+C)^2} + 2D\lambda}{2\left[A + \frac{B}{\lambda^2+C} + D\lambda^2\right]}\Delta\lambda \\ &\approx \pm 0.002 \end{aligned} \tag{C.20}$$

As such, the uncertainty in the product of $n_o^3 r_{22}$ is,

$$\begin{aligned} \Delta n_o^3 r_{22} &= \sqrt{\left(\frac{\Delta m}{m}\right)^2 + \left(\frac{\Delta\lambda}{\lambda}\right)^2} \times n_o^3 r_{22} \\ &\approx \pm 0.03 \times 10^{-11}\ \mathrm{mV}^{-1} \end{aligned} \tag{C.21}$$

Thus, the uncertainty in the r_{22} is

$$\begin{aligned} \Delta r_{22} &= \sqrt{3\left(\frac{\Delta n_0}{n_0}\right)^2 + \left(\frac{\Delta n_o^3 r_{22}}{n_o^3 r_{22}}\right)^2} \times r_{22} \\ &\approx \pm 0.085 \times 10^{-12}\ \mathrm{mV}^{-1} \end{aligned} \tag{C.22}$$

Generally, due to the difficulty in determine the electro-optical coefficient of crystals, the electro-optical coefficient is usually reported to two significant figures. Since our statistical calculation is still less than that, we take the nearest ceiling of the uncertainty of $\pm 0.1 \times 10^{-12}\ \mathrm{mV}^{-1}$. This is done similarly to the product of $n_o^3 r_{22}$ - rounding up its uncertainty to 1 decimal place.

C.6 Other Experimentally Assigned Uncertainties

The lowest division for the angular position of the polarizer is 2°, thus the uncertainty and error bar of the angular positions is ±1°. The lowest division that can be read off from the oscilloscope directly is used to give the uncertainties for the rise and fall times of the optical response and the electrical signal. The uncertainty of the high voltage power supply is taken to be ±0.1 V.

Appendix D

Pictures of Experimental Setups

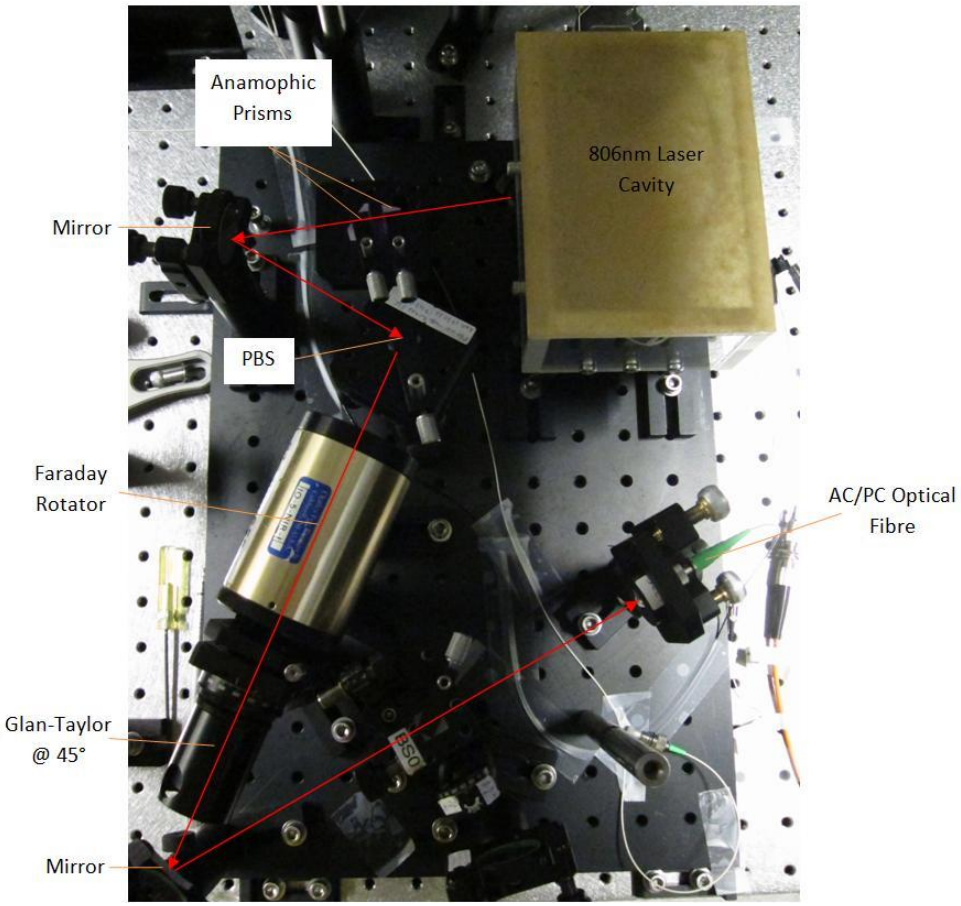

Figure D.1: The external laser cavity setup. The red arrows show the propagation of the laser beam.

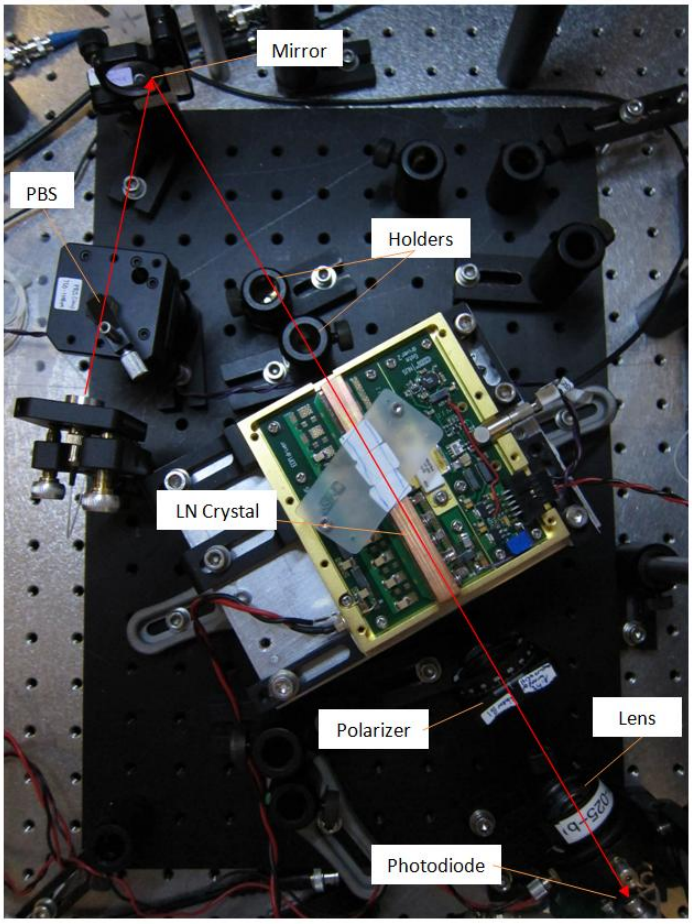

Figure D.2: The setup for LN crystal characterization. The empty holders allow us to shift the polarizers and pinholes during the alignment of the crystal.

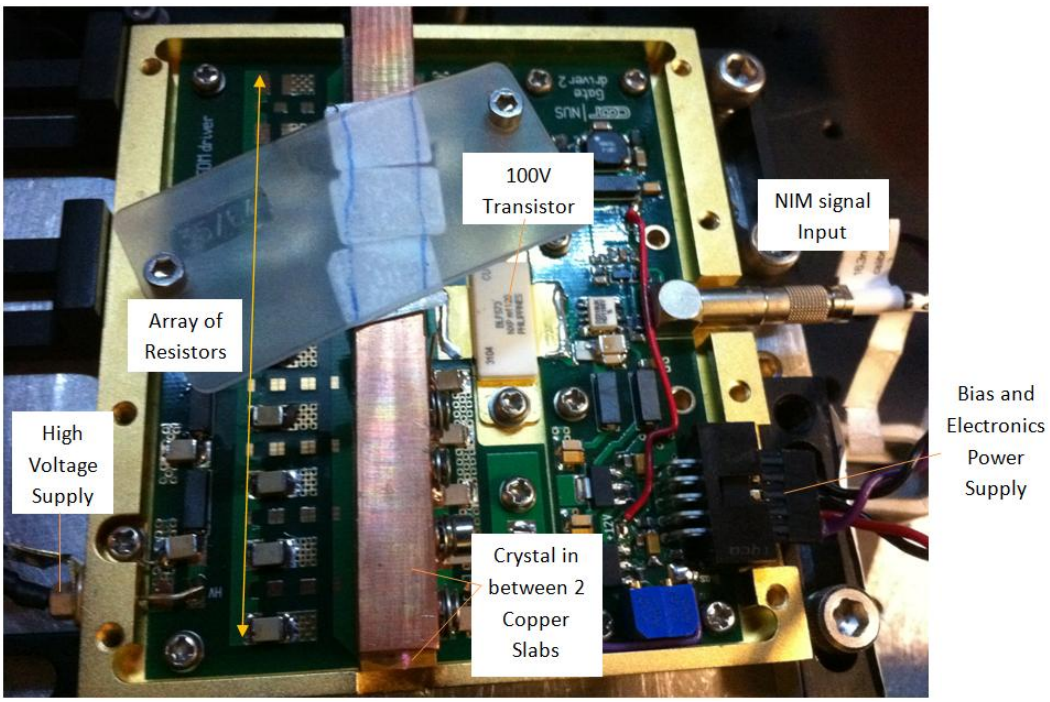

Figure D.3: A close up on the some of the important component of the electronic circuit on the holder. The two copper slabs are not considered during the initial design of the holder. Thus, the cover is not shown in this figure.

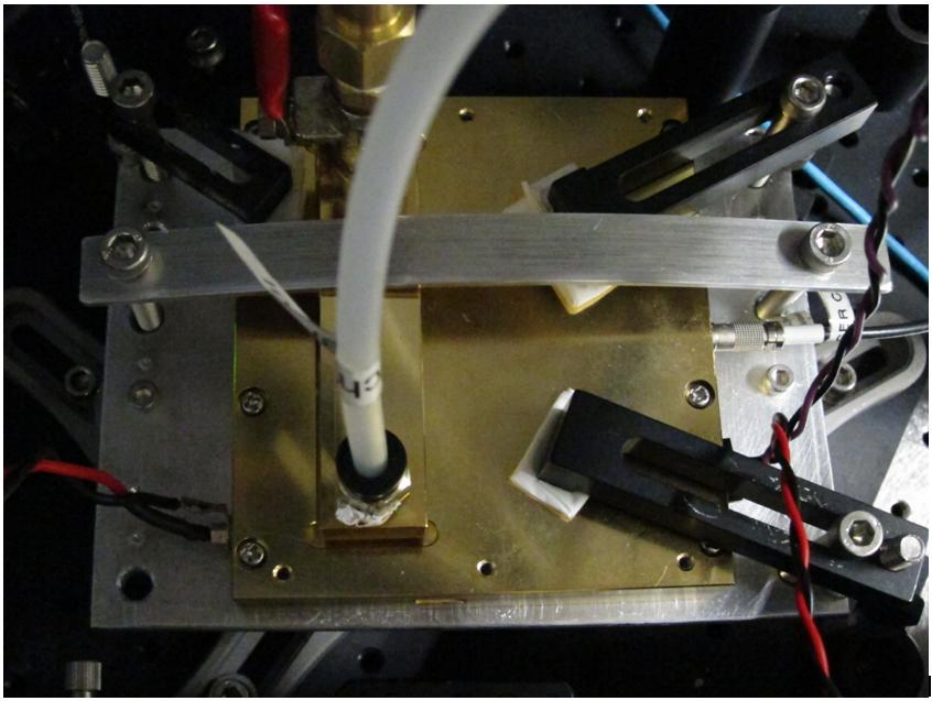

Figure D.4: The covered crystal holder without the two copper slabs. The water chiller component is placed directly above the array of resistors to remove the any heat generated.

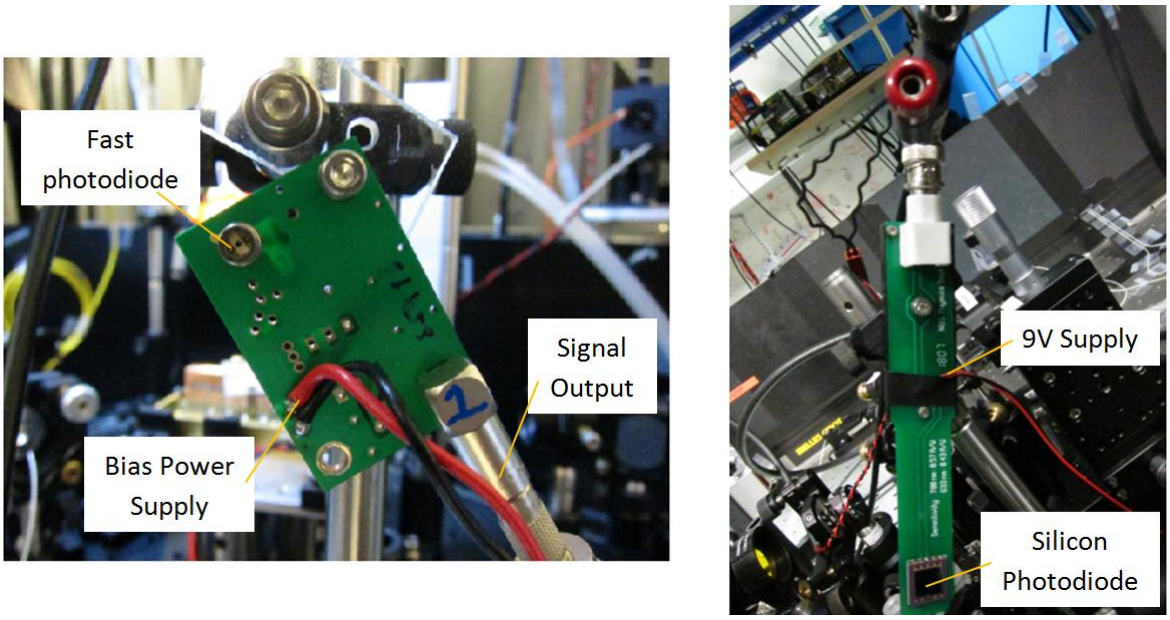

Figure D.5: The detectors used in characterization of the LN crystal. Left: Fast photodiode for registering fast optical response from the crystal. Right: The Silicon photodiode using the 9V supply.